VYSOKÉ UČENÍ TECHNICKÉ V BRNĚ

BRNO UNIVERSITY OF TECHNOLOGY

FAKULTA STROJNÍHO INŽENÝRSTVÍ

ÚSTAV MECHANIKY TĚLES, MECHATRONIKY A BIOMECHANIKY

FACULTY OF MECHANICAL EGINEERING

INSTITUTE OF SOLID MECHANICS, MECHATRONICS AND BIOMECHANICS

TOWARDS PATIENT SPECIFIC ASSESSMENT OF RUPTURE RISK OF ABDOMINAL AORTIC ANEURYSM

(COMMENTED SET OF PAPERS)

HABILITAČNÍ PRÁCE

HABILITATION THESIS

AUTOR PRÁCE
AUTHOR

Ing. STANISLAV POLZER, Ph.D.

BRNO 2017

Acknowledgement

I would like to express my gratitude to all my colleagues at Brno University of Technology namely Prof. Jiří Burša, Ph.D., Ing. Pavel Skácel, Ph.D., Ing. Kamil Novák, Ing. Vojtěch Man and Ing. Martin Slažanský. I am also thankful to my collaborators from the clinical area Prof. Robert Staffa, Ph.D., Prof. Markéta Hermanová Ph.D., MUDr. Robert Vlachovský, Ph.D., MUDr. Luboš Kubíček, MUDr. Michal Tichý and MUDr. Lukáš Lambert, Ph.D. Research is in principle a collaborative work and I am lucky I can share my ideas with those people as well as receive a priceless feedback from them which keeps me on the track.

I would also like to thank prof. T. Christian Gasser, Ph.D. from Royal Institute of Technology, Stockholm who kindly reviewed most of my papers and also provided valuable feedback which dramatically improved my outputs.

Last but not least I would like to thank my family which showed endless patience and understanding. I could not do my research without their support and love.

1 Summary

Abdominal aortic aneurysm (AAA) is a pathological local dilatation of human aorta which affects mostly older male patients. Existence of AAA is mostly asymptomatic and does not bring any difficulties to the patient but its danger is in its potential to rupture. AAA rupture is a catastrophic outcome which is associated with about 50% mortality and excessive financial expenses when treated. On the other hand not all AAAs rupture so there is an intensive research with the aim to find out a reliable criterion how to distinguish safe AAAs from the risky ones. The currently used criterion of maximal diameter is not reliable so many researchers focus on proposing some wall stress based criterion instead. This is also core of the author's research.

This thesis is a commented list of papers and is structured as follows. At first the introduction to the field of arterial biomechanics is provided for non specialized readers. Structure of aortic wall and mechanical behavior of its components is followed by a summary of most important constitutive models used in numerical simulations and chapters dedicated to pathological changes in aorta due to ageing and presence of AAA. Final chapter of this part describes the wall stress in AAA and its potential to predict rupture of AAA.

Main part of the thesis consists of full texts of Author's publications. Initially, the summary of citations for all author's publications is provided together with other scientometric parameters. Each full text is completed by a chapter of Author's comments where the motivation and main results are discussed in detail.

Content

2 Author's list of publications

A. **Polzer S**, Bursa J, Gasser TC, Staffa R, Vlachovsky R. A numerical implementation to predict residual strains from the homogeneous stress hypothesis with application to abdominal aortic aneurysms. Ann Biomed Eng 2013;41:1516–27. doi:10.1007/s10439-013-0749-y.

B. **Polzer S**, Christian Gasser T, Bursa J, Staffa R, Vlachovsky R, Man V, et al. Importance of material model in wall stress prediction in abdominal aortic aneurysms. Med Eng Phys 2013;35. doi:10.1016/j.medengphy.2013.01.008.

C. **Polzer S**, Gasser TC, Forsell C, Druckmullerova H, Tichy M, Staffa R, et al. Automatic identification and validation of planar collagen organization in the aorta wall with application to abdominal aortic aneurysm. Microsc Microanal 2013;19. doi:10.1017/S1431927613013251.

D. **Polzer S**, Gasser TC, Novak K, Man V, Tichy M, Skacel P, et al. Structure-based constitutive model can accurately predict planar biaxial properties of aortic wall tissue. Acta Biomater 2015;14. doi:10.1016/j.actbio.2014.11.043.

E. **Polzer S**, Gasser TC. Biomechanical rupture risk assessment of abdominal aortic aneurysms based on a novel probabilistic rupture risk index. J R Soc Interface 2015;12. doi:10.1098/rsif.2015.0852.

F. Novak K, **Polzer S**, Tichy M, Bursa J. Automatic Evaluation of Collagen Fiber Directions from Polarized Light Microscopy Images. Microsc Microanal 2015;21. doi:10.1017/S1431927615000586.

G. Khan S, Verma V, Verma S, **Polzer S**, Jha S. Assessing the potential risk of rupture of abdominal aortic aneurysms. Clin Radiol 2015;70:11–20. doi:10.1016/j.crad.2014.09.016.

H. Slazansky M, **Polzer S**, Man V, Bursa J. Analysis of Accuracy of Biaxial Tests Based on their Computational Simulations. Strain 2016;52. doi:10.1111/str.12205.

2.1 Commentary to references

The references in this thesis are structured as follows: Author's publications published after author's Ph.D. defense are listed in chapter 2 and Author's name is marked bold. This publications are referenced by capital letters bold **A, B**, etc. in the thesis. On the contrary, Author's publications published before his Ph.D. defense are listed together with other references in chapter 7. For better identification the Author's name is also marked bold there. These publications are referenced by numbers in brackets [1], [4-6] etc. in the thesis. Both lists of references are also used in the comments to each of the Author's publication which are formatted as rest of this thesis while full texts of published papers (not included in the online version due to copyright restrictions) are formatted differently according to the style of each journal and also the related references are listed directly at the end of each manuscript.

3 Introduction

This thesis is focused on numerical prediction of rupture of abdominal aortic aneurysm (AAA) As an outcome of diseased human aorta. However for understanding of important pathophysiology of aneurysmatic aorta, it is necessary to describe the structure and physiology of healthy aorta first.

Aorta is the largest artery in mammalian body. It falls in to group of so called elastic arteries and plays a key role in distributing blood from the heart towards more peripheral parts of the body. Due to its closeness to the heart it is mechanically loaded by high pulsatile pressure during the cardiac cycle which affects its structure optimized to sustain such loading. From a mechanical point of view it contains three key structural components which determine its mechanical properties.

3.1 Constituents of aortic wall

3.1.1 Elastin

First of them is elastin. It is very a compliant sub-structure created from tropoelastin protein which is arranged in complex 3D structure containing mutually connected lamellae [1]. Human aorta contains about 70 lamellae in thoracic part and this number decreases to about 30 lamellae in the abdominal part of the aorta[2]. Elastin (tropoelastin) is expressed by smooth muscle cells mainly during development phase and it has a long half-life of about 40 years[3, 4]. Volume fraction of elastin in healthy aorta is about 25%[5].

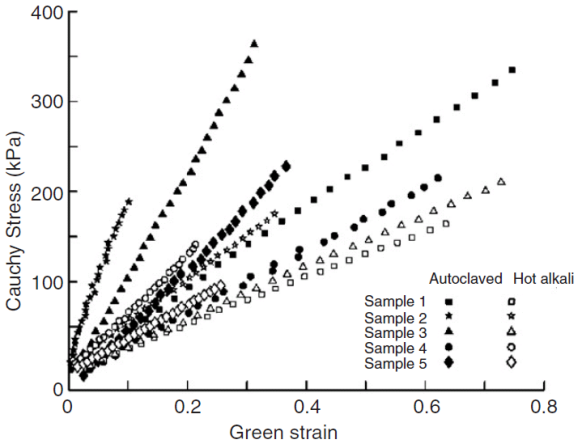

Figure 1 Mechanical response of arterial elastin obtained from porcine aorta by two different chemical procedures (irrelevant for purposes of this thesis).It is clearly shown that mechanical response is linear. Reprint from [6]

Despite its complex structure, elastin has practically isotropic and linear mechanical response in the Cauchy stress vs. Green strain space[6, 7] as demonstrated in Figure 1. Therefore its contribution to total mechanical response of the arteries is often[6, 8–10] modeled by Neo-Hookean constitutive model given by the following strain energy density function (SEDF):

$$\Psi = c_{10}(I_1 - 3)\,, \tag{1}$$

where c_{10} is a material constant and I_1 refers to the first invariant of the right Cauchy-Green deformation tensor.

3.1.2 Collagen

Collagen is the most abundant protein in mammalian body[11]. 28 different types of collagen have been identified up to now[11]. Out of these the type I collagen is by far the most common in the arterial wall (minor portion is also type III collagen). Therefore only type I will be described in this section.

Three left-handed polypeptidic chains of procollagens are joined and create a right-handed triple helix of tropocollagen which is about 300 nm long and 1.5nm in diameter. Tropocollagens form fibril where each tropocollagen overlaps its neighbor by certain length forming so called D-unit[12]. The D unit consists of two parts called “Overlap” and “Gap”. The cross section of the fibril contains 5 tropocollagens in the Overlap section and 4 in the Gap section. The D unit is visible by electron microscopy[13] as shown in Figure 2. Finally, the collagen fibrils are packed into collagen fiber which is the largest collagen unit in arterial wall. Individual fibrils are connected into the collagen fiber by cross links created by proteoglycans. This cross linking is responsible for increase of collagen mechanical properties such as stiffness and strength during maturation[11]. Stiffness of the straight matured collagen fiber is in the order of GPa[14]. It is noted that collagen fibers can form even larger structures such as fiber bundles and fascicles but these are present in tendons and therefore not discussed here.

Unlike elastin, arterial collagen has a half-life of about 60-70 days [15] which can be however reduced up to 4 times in case of injury or disease [15]. It is expressed by smooth muscle cells in media (arterial structure is described in chapter 3.2) and by fibroblasts in adventitia during the whole life and its volume portion in the infrarenal aorta is about 40% [5].

It is also important to mention that collagen in arterial wall is not in a form of straight fibers but rather as a dense mesh of dispersed and wavy fibers. Both of these properties determine the global mechanical response of arterial wall as described below.

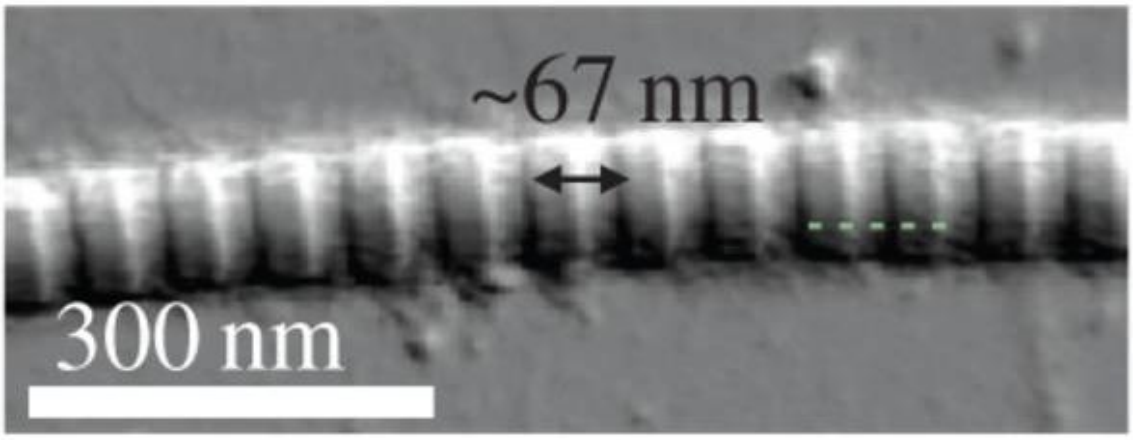

Figure 2 Real image of collagen fibril showing the D unit (marked by its size of 67nm) pattern. Reprint from[13]

Waviness of the collagen fibers can be characterized by several parameters. Here, a definition from other authors [16, 17] is adopted so the waviness w is defined as a ratio $w = \frac{L}{L_0}$, where L is the true length of the fiber and L_o is the straight distance between fiber's end points. Consequently straight fiber has $w = 1$, fiber with its L longer by 20% compared to L_o would be characterized by $w = 1.2$ and so on. Under normal conditions, the collagen is highly undulated in the adventitia and all the load is carried by media which contains much less undulated collagen [17, 18, **D**]. The waviness of medial collagen is less than $w < 1.1$ [18]. Typical structure of collagen fibers in the aortic adventitia and media can be seen in Figure 3A and B respectively. The waviness of adventitial collagen demonstrates itself during deformation by typical "heel" region where the stiffness gradually increases as more and more collagen fibers are straightened out as shown in Figure 6 and also in literature[20]. For more information see also chapter 0 of this thesis.

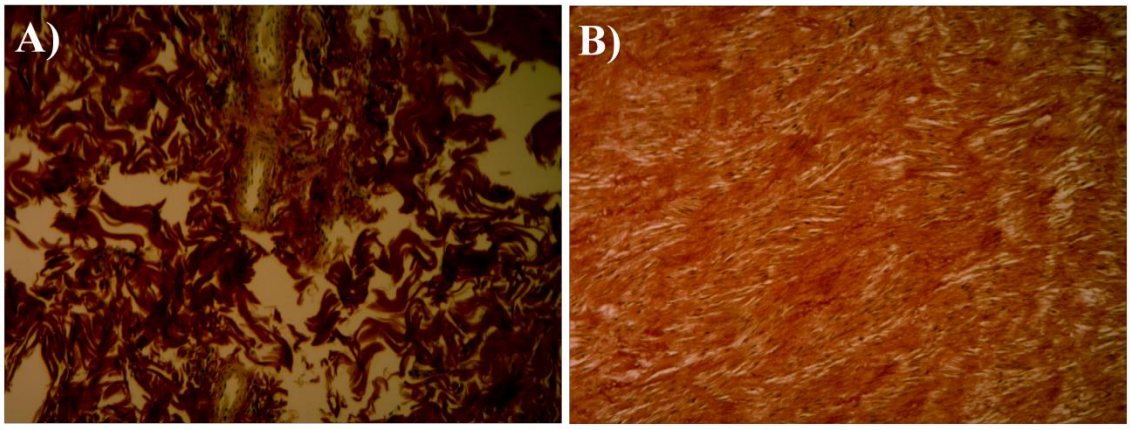

Figure 3 Typical collagen (red) structure in porcine aortic wall. Collagen in adventitia A) is much more wavy compared to collagen in media B). Black dots refer to smooth muscle cells. Magnification 100x, stained by Picrosirius red.

Another key property of collagen fibers in the arterial wall is their orientation. For a long time it was believed that collagen forms two families of fibers which have roughly symmetrical declinations from the circumferential direction[8, 9, 21, 22]. More recently, when large amount of samples has been analyzed, this statement has been refined to one family of fibers with a significant dispersion[23, **D**]. This is discussed in chapter 4.5 in greater detail and illustrated in Figure 2 in Author's publication [**D**] attached in chapter 4.5.2 where this observation is visualized.

3.1.3 Cells

Collagen and elastin form most of so called extracellular matrix. Besides that there are also different types of cells in the aortic wall. Here only two types important for mechanical properties and/or remodeling of arterial wall will be discussed; smooth muscle cells (SMC) and fibroblasts.

SMC are located in the arterial media and they are responsible for remodeling of the arterial wall (in term of weeks) and active regulation of arterial stiffness (in term of 10s of seconds). Both responses are thought to be processed via mechanotransduction when mechanical stimulus (such as elevated blood pressure) starts the SMCs reaction [24] which is in short term relaxation/contraction. By changing its size a SMC also changes the waviness of surrounding collagen which results in either increase of arterial stiffness when SMCs contract (as shown in Figure 4) or its decrease when they relax. Volume fraction of SMCs in abdominal aorta is about 23%[5]. Fibroblasts do not have this regulation function because they are surrounded by much more wavy collagen in the adventitia (see Figure 3).

In long term, both SMCs and fibroblasts are responsible for collagen decomposition and secretion (=turnover). Arterial adaptation to aging and/or diseases depends on this capability[24].

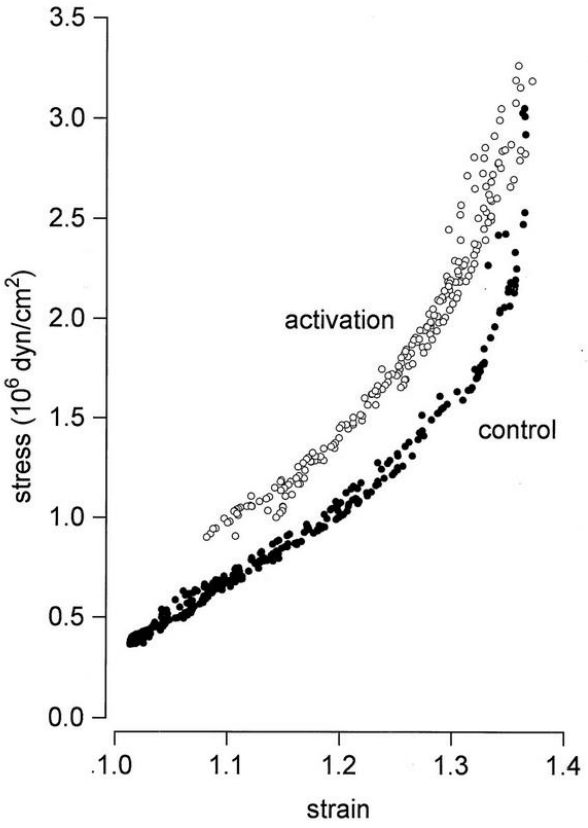

Figure 4 Stress-strain curves of dogs aortas when SMCs are under normal conditions and activated (=contracted). Reprint from [25]

3.2 Aortic structure

So far, the principal constituents of the aortic wall have been described. However they are not distributed in the arterial wall randomly but create three layers with unique structure and role they play in the physiology of the aorta.

3.2.1 Intima

Intima is the most inner layer of artery. It has a monolayer of endothelial cells which creates the arterial lumen and separates the blood from other parts of the artery which are trombogenic. The endothelial cells sit on a net of collagen fibers oriented mainly in axial direction[26]. However in about 100μm depth from the luminal side the axial orientation changes abruptly to circumferential orientation[26]. It is not clear whether this change occurs still in the intima or it is already in the media since thickness of the intimal layer is about 6% of the healthy artery total

thickness[27] but it can grow up to 27% in aged arteries[28]. Intima is separated from media by membrana elastica interna which is an elastin membrane.

3.2.2 Media

Aortic media creates most of the artery's volume. It consists of various number of medial lamellae created by elastin membranes, SMCs and collagen fibers [1] oriented mainly circumferentially with rather low waviness[18] (see Figure 3B). The main orientation of collagen fibers is maintained across the media but it is less and less apparent (more dispersed fibers) with increasing distance from lumen [**D**]. Drawing of few medial lamellae can be seen in Figure 5. Media carries the load caused by blood pressure under normal loading conditions. Membrana elastica externa separates media from the outer layer of the artery which is adventitia.

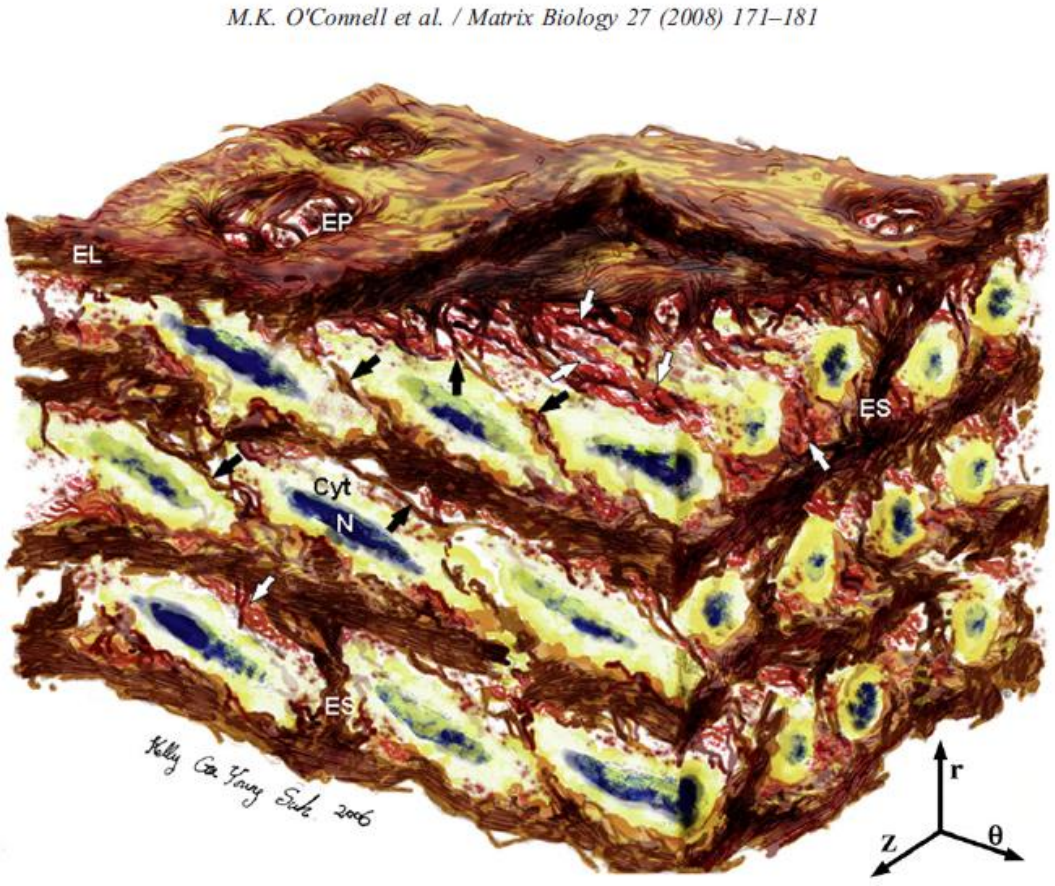

Figure 5 Artistic sketch of rat aortic medial microstructure. Elastin is colored brown and it forms elastic lamellae (EL), dense network of interlamellar elastin fibers (IEFs shown with black arrows), elastin struts (ES), and reinforced elastin pores (EP). SMCs (marked yellow) with elliptical nuclei (N-marked dark blue) are oriented circumferentially with radial tilt. Collagen fibers (colored red, marked by white arrows) are arranged in layers of parallel bundles oriented predominantly circumferentially. Image dimensions (θ×Z×r where r indicates radial, Z axial, and θ circumferential directions) are 80 μm×60 μm×45 μm, with lumen surface at the top. Reprint from [1].

3.2.3 Adventitia

Adventitia is the outer arterial layer which contains mostly wavy collagen fibers and fibroblasts ensuring its turnover procedure. Concentration of fibroblasts is however much lower compared to SMCs in media. That is given by the extensive distance from the blood flow which limits the oxygen and nutrients delivery into this layer. In large arteries, the aortic wall thickness is as big that the adventitia contains also vasa vasorum (small diameter arterioles) which provide a proper blood supply[29]. Their concentration is larger in the ascending aorta and decreases towards the thoracic and abdominal aorta as the wall thickness also decreases.

Adventitia also serves as a protective layer which prevents artery from damage under supraphysiological loading [**D**]. Adventitial collagen also fixates the aorta's proper position with respect to other organs.

3.3 Mechanical response of healthy aorta and its constitutive modeling

A lot of effort has been put into constitutive modeling of the structure of aorta described above. This is motivated by a need to understand the mechanism how the load is carried by the aortic wall, what constituents are responsible for a particular observed global behavior (axial pre-strain, anisotropy, strain stiffening etc.)

Globally, the mechanical response of arteries to loading is highly nonlinear and also anisotropic (see Figure 6 and Figure 7) with the ratio of circumferential to axial stresses being about 2 under a given stretch. The anisotropy is believed to originate in arrangement of collagen fibers which are primarily oriented in the circumferential direction [22, 23, **D**]. On the other hand, the collagen waviness (see also chapter 3.1.2) is believed to be responsible for the nonlinear behavior with typical regions such as "Toe region" characterized by low stiffness, "high load" region with high stiffness at the end of stress –strain curve and a "heel region" in the middle of the stress-strain curve where the stiffness increases gradually. Several constitutive models have been proposed in order to capture this known behavior. Without attempting to include all of them, a description of the most relevant constitutive models is now provided. It is noted that incompressible definitions of all of the models are discussed only.

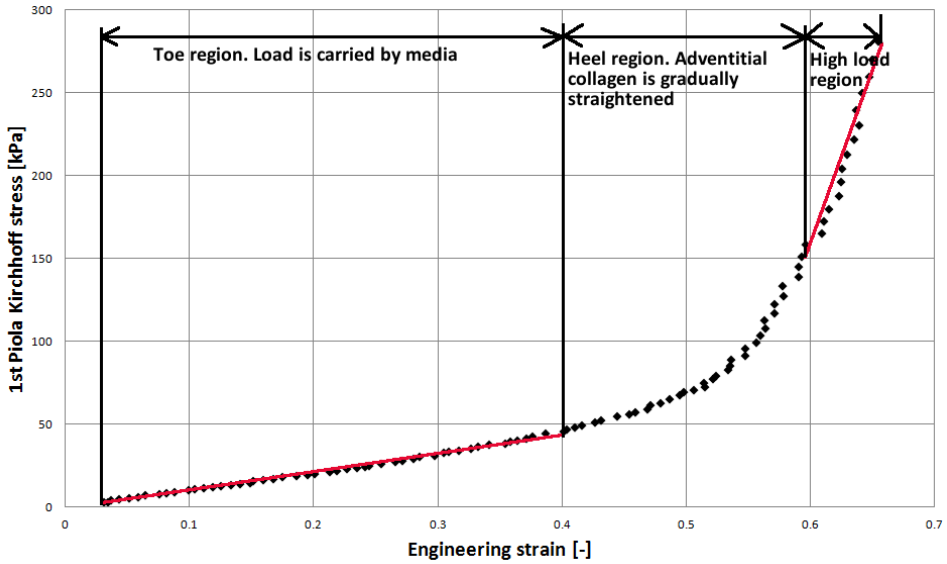

Figure 6 Typical uniaxial response of healthy porcine aortic wall specimen subjected to uniaxial tensile test. Initially, the response is almost linear and all the load is carried by media. This is called the "Toe region". Then the adventitial collagen becomes gradually straightened which result in inrease of stifness. Finally, most fo the collagen is straight so the response is again almost linear. This is called high load region.

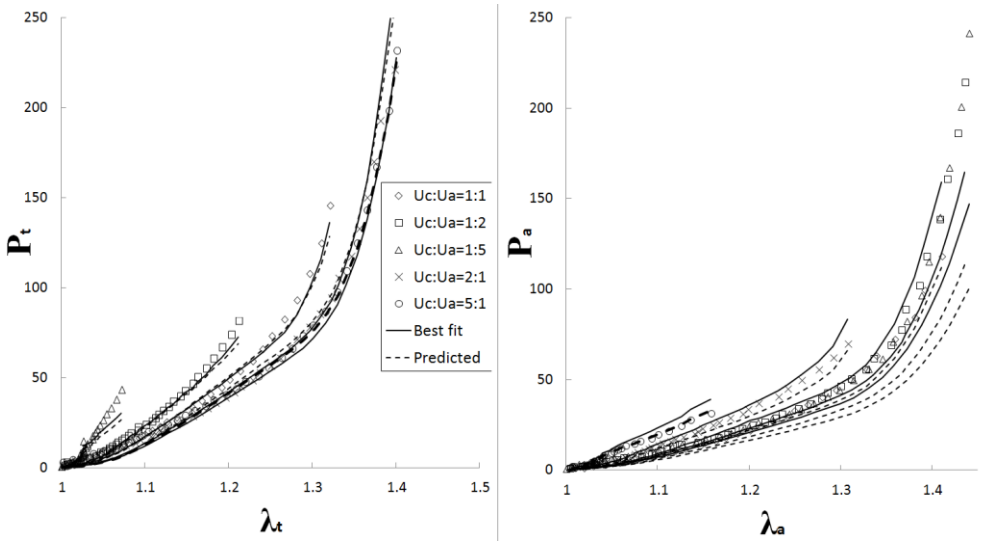

Figure 7 typical biaxial response of healthy aortic wall specimen subjected to various planar biaxial tests showing its anisotropy. P refers to 1st Piola Kirchhoff stress, λ represents the stretch, subscript a means axial direction while subscript t is for circumferential direction. Experimental data are displayed by symbols while best fit and predicted response using Martuffi Gasser model is plotted by solid and dashed lines respectively.

3.3.1 Fung model

This model has been originally derived in 1979 [30] and it has SEDF as follows:

$$\Psi = \frac{c}{2}(e^{Q} - 1),$$

$$Q = b_1 \cdot E_{CC}^2 + b_2 \cdot E_{ZZ}^2 + b_3 \cdot E_{RR}^2 + 2b_4 \cdot E_{CC} \cdot E_{ZZ} + 2b_5 \cdot E_{RR} \cdot E_{ZZ} + 2b_6 \cdot E_{CC} \cdot E_{RR} \quad (2)$$

where c is a stress-like material parameter, b_1 through b_6 are dimensionless parameters and E_{ii} are diagonal components of Green-Lagrange strain tensor **E.** Although this model can usually accurately capture biaxial response of arterial wall its definition is not suitable for implementation into finite element (FE) software because it cannot describe shear deformation. Three decades later it was generalized in a way suitable for use in FE software[31]. It is a typical example of so called phenomenological constitutive models which do not attempt to relate individual parameters to known structural information on aortic wall.

3.3.2 Holzapfel Gasser Ogden (HGO) model

Compared to Fung model discussed above, the HGO model [8] is a more recent (published in 2000) and extremely widely used model (over 2000citations according to Google scholar). Its SEDF is as follows:

$$\Psi = \Psi_{iso} + \Psi_{aniso} = \frac{c}{2}(I_1 - 3) + \sum_{i=1,2} \frac{k_1}{2 \cdot k_2}\left(e^{k_2 (I_{4i}-1)^2} - 1\right), \quad (3)$$

where c is a stress-like material constant describing the isotropic response of the tissue, k_1 is a stress-like constant defining the stiffness of collagen fibers, and k_2 refers to collagen stiffening during deformation. I_1 is the first invariant of the right Cauchy-Green deformation tensor **C**, $I_{41} = \boldsymbol{a_{01}} \cdot \boldsymbol{C a_{01}}$ and $I_{42} = \boldsymbol{a_{02}} \cdot \boldsymbol{C a_{02}}$ are invariants related to two families of fibers; here $\boldsymbol{a_{01}} = (cos\ \varphi, sin\ \varphi\ , 0)^T$ and $\boldsymbol{a_{02}} = (-cos\ \varphi, sin\ \varphi, 0)^T$, with φ representing the angle between each fiber family and the circumferential direction.

Unlike the previous model this one is more inspired by the observed mechanical response of individual constituents of arterial wall (see chapter 0). The authors of HGO model assumed its isotropic response should represent elastin (see chapter 3.1.1) and the anisotropic part mimics two families of collagen fibers declining symmetrically from the circumferential direction according to histological observations relevant in that time.

Despite its indisputable quality the HGO model has also several limitations. First, it neglects the dispersion of collagen fibers around the preferential direction which is consistently reported in literature [22, 23, 26, **D**]. Second, the concept of two families of fibers is gradually impeached by new histological observations (see chapter 3.1.2). Finally, it takes the waviness of fibers into account only phenomenologically by assuming exponential stiffening; this simplification makes this model often ill-conditioned especially when material response outside the tested range is predicted. Due to these limitations, the author of this thesis prefers to include the HGO model into a family of phenomenological models; despite he is aware this might be a controversial claim.

3.3.3 Four fiber family model

The above presented model served as a basis for definition of another constitutive model by Baek et al.[32, 33] with the following SEDF:

$$\Psi = \Psi_{iso} + \Psi_{aniso} = \frac{c}{2}(I_1 - 3) + \sum_{i=1}^{4} \frac{k_{1i}}{4 \cdot k_{2i}} \left(e^{k_{2i}(I_{4i}-1)^2} - 1 \right) \tag{4}$$

where 4 families of fibers with different mechanical properties (represented by parameters k_{1i} and k_{2i} for the i-th family of fibers) are introduced. Invariants $I_{4i} = \boldsymbol{a_{0i}} \cdot \boldsymbol{C a_{0i}}$ related to each family of fibers are here defined similarly to HGO model (see chapter 3.3.2) and the directions of an individual family of fibers are given by $\boldsymbol{a_{01}} = (0, 1, 0)$ and $\boldsymbol{a_{02}} = (1,0, 0)$, $\boldsymbol{a_{01}} = (sin\,\varphi, cos\,\varphi, 0)$ and $\boldsymbol{a_{02}} = (sin\,\varphi, -cos\,\varphi, 0)$, with φ representing the angle between each fiber family and the circumferential direction. In other words, this model adds two more fiber families to the above HGO model, one of them with fibers heading in circumferential direction and another one in axial direction. The increasing number of families of fibers can be interpreted as an approximation of fiber dispersion since four families of fibers were never observed in arterial wall.

3.3.4 Gasser model

This model is derived by the same group of authors as HGO model in 2006 [9]. This modification of HGO model was motivated by an effort to take the known dispersion of fibers into consideration. The SEDF of this model is similar to eq. (3):

$$\Psi = \Psi_{iso} + \Psi_{aniso} = \frac{c}{2}(I_1 - 3) + \sum_{j=1,2} \frac{k_1}{2 \cdot k_2} \left(e^{k_2 {E_i}^2} - 1 \right), \tag{5}$$

where the newly introduced parameter $E_i = \mathbf{H_i}: \mathbf{C} - 1$ represents average strain measure of fibers. Here, the generalized structure tensor $\mathbf{H_i} = \kappa \mathbf{I} + (1 - 3\kappa)(\boldsymbol{a_{0i}} \otimes \boldsymbol{a_{0i}})$ contains the parameter κ which describes the fiber dispersion around their mean direction and $\boldsymbol{a_{0i}}$ holds the same meaning as in the HGO model (see chapter 3.3.2).

3.3.5 Rodriguez model

This model originates from another attempt to include dispersion[34] but it is more general with the following SEDF:

$$\Psi = \Psi_{iso} + \Psi_{aniso} = \frac{c}{2}(I_1 - 3) + \sum_{i=1}^{2} \frac{k_{1i}}{2k_{2i}} \left(e^{k_2 \cdot [(1-\rho)(I_1-3)^2 + \rho(I_{4i} - I_{4i0})^2]} - 1 \right) \qquad (6)$$

where two families of fibers with different mechanical properties (represented by parameters k_{1i} and $k_{2i}$for each family of fibers) are assumed. The isotropic response is again simulated by Neo-Hookean material with material constant c (shear modulus). The dispersion of fibers is represented by parameter ρ which is defined in range from 0 (which defines isotropic exponential response of fibers) to 1 (which means no dispersion). Besides that, it contains also two parameters I_{4i0} representing fiber stretch threshold. No fiber stress is generated if stretch is below this threshold below which no fiber stress is generated in the concerned family of fibers. On the other hand the gradual increase of stiffness during deformation of arterial wall is a consequence of gradual straightening of fibers with different waviness. Therefore, the parameters I_{4i0} should be understood as a stretches at which the least wavy fiber becomes completely straight. Further increase of stiffness is in this model captured only implicitly by the exponential stiffness function for fibers.

3.3.6 Martufi-Gasser model

More recently, Martufi and Gasser[10] proposed a more structurally motivated constitutive model. The mentioned model is characterized by the following SEDF:

$$\Psi = \Psi_{iso} + \Psi_{aniso} = \frac{c}{2}(I_1 - 3) + \int_{\omega} \rho_d \psi_f^{a_0}(\mathbf{C}, \mathbf{a_0}) d\varpi \qquad (7)$$

where $\psi_f^{a_0}$ is the contribution of fibers oriented in $\mathbf{a_0}$ direction, ω is the domain of all possible fiber directions (typically a unit sphere or a unit circle for in plane fiber distributions). Then the stress σ in the given direction can be estimated as:

$$\frac{\partial \psi_f^{a_0}}{\partial I_4} = \frac{1}{2\lambda^2}\sigma\big(\lambda(\mathbf{a_0})\big) \tag{8}$$

with I_4 defined as in chapter 3.3.2. Then, the specific constitutive model for uniaxial response of fibers follows the paper by Martufi and Gasser paper[10]:

$$\sigma(\lambda) = \begin{cases} 0, & 0 < \lambda \leq \lambda_{\min} \\ \frac{2k}{3\Delta\lambda^2}\lambda(\lambda - \lambda_{\min})^3, & \lambda_{\min} < \lambda \leq \bar{\lambda} \\ k\lambda\left[\lambda - \frac{2(\lambda-\lambda_{\max})^3}{3\Delta\lambda^2} - \bar{\lambda}\right], & \bar{\lambda} < \lambda \leq \lambda_{\max} \\ k\lambda\big(\lambda - \bar{\lambda}\big), & \lambda_{\max} < \lambda < \infty \end{cases} \tag{9}$$

with $\Delta\lambda = \lambda_{\max} - \lambda_{\min}$ and $\bar{\lambda} = (\lambda_{\max} + \lambda_{\min})/2$, and k denoting the stiffness of the collagen-fibril proteoglycan complexes (CFPG-complex). This constitutive model assumes a triangular distribution of fiber waviness which is of course a simplification. However, it does not negatively affect the capability of this model to capture the known biaxial behavior of healthy aorta as demonstrated in Figure 7 and in [**D**].

3.4 Effect of Ageing on the aortic structure

Significant changes occur in the structure and physiology of aorta during ageing. Globally it is observed that the diameter and stiffness are increasing, while the axial pre-strain is decreasing in consequence of age.

3.4.1 Aortic diameter during ageing

Aortic diameter is known to increase not only during ontogenesis [36, 37] but also during ageing[36]. It has been shown that diameter of healthy male aorta increases by some 30% between ages of 25 and 70 years[37] (i.e. from 17mm to 22mm). Another study showed a smaller but still statistically significant increase of aortic diameter[38] (1mm in a group of veterans from 50 to 79 age). Finally, it has been shown that the undeformed outer abdominal aortic diameter also increases from some 8mm in 10years old up to 17mm for 80years old humans[39]. All of these observations correspond to the observed decrease of tissue dry mass including elastin and collagen [40] and increase of blood pressure during ageing[41].

3.4.2 Arterial stiffness during ageing

The arterial stiffness increases during ageing as well. This can be demonstrated by increase of pulse wave velocity (PWV) with increasing age[42, 43]. PWV increases about 3times from 5m/s in 20years old humans to some to some $15ms^{-1}$ in 90years old[43, 44]. The relation between mechanical properties and PWV is called Moens-Korteweg equation:

$$PWV = \sqrt{\frac{E \cdot h}{d_a \rho}} \tag{10}$$

where E refers to Young's modulus of the artery, h is its thickness, d_a is the diameter of the artery and ρ_b is the density of the blood. Although this equation has been derived for tubes with constant cross section made of a linear material, and the simplified shape (10) neglects the compressibility of the liquid, the trends predicted by it are usable also in arterial mechanics, where material nonlinearity is often neglected (even in current studies e.g.[45]) when behavior under a narrow pressure range (typically from systolic to diastolic pressure) is investigated. Eq. (10) shows that the observed increase of PWV might be caused either by a diameter decrease (not true — up to 30% diameter increase was observed[37]), blood density decrease (there is no evidence for that), wall thickness increase (24% increase have been observed between ages 50 and 80years[46]) or Young's modulus increase. Since the changes of aortic diameter and wall thickness largely compensate each other, the Young's modulus increase is almost exclusively responsible for the increase of PWV during ageing. Here it must be pointed out that the clinical practice uses more often the term "Stiffness" β [36, 47] defined as follows:

$$\beta = \frac{ln\left(\frac{p_{syst}}{p_{diast}}\right)}{\frac{D_{syst} - D_{diast}}{D_{diast}}} \tag{11}$$

where $p_{syst}$and p_{diast} mean systolic and diastolic pressures respectively, while D_{syst} and D_{diast} refer to the arterial diameters under systolic and diastolic pressures, respectively. This definition of stiffness also depends implicitly on the material of the artery since D_{syst} is a consequence of p_{syst}, Young's modulus and D_{diast}. However β does not have same units as stiffness in engineering practice (where it equals either Young's modulus or, for nonlinear materials, a tangent of stress-strain curve at its certain point), thus one must be careful which stiffness he talks about.

3.4.3 Axial pre-strain during ageing

Decrease of axial pre-strain is another important change which is observed in ageing aortas. The pre-strain which is about 40% in humans turning 18 years decreases then nonlinearly and it almost vanishes for people above 70 years[48]. It is noted that axial pre-strain as well as its decrease during ageing strongly depends on the type of artery. For instance, a significant axial pre-strain of up to 25% has been observed in iliac arteries (one of the aorta major branches) even at elder patients[49].

3.5 Abdominal aortic aneurysm (AAA)

Structure of a normal aorta and the changes ongoing in it due to ageing have been described in this thesis so far. Unfortunately, aorta can be also subjected to pathological changes which lead to diseases such as atherosclerosis or AAA.

AAA is characterized by a gradual increase of diameter of abdominal aorta which starts to dilate faster than the rest of the aorta, forming a typical bulge as shown in Figure 8. However, the aortic enlargement itself is not pathological[36], so a widely accepted definition states that AAA occurs at infrarenal aorta if its maximal diameter is by at least 50% greater compared to the non dilated part of the aorta[50].

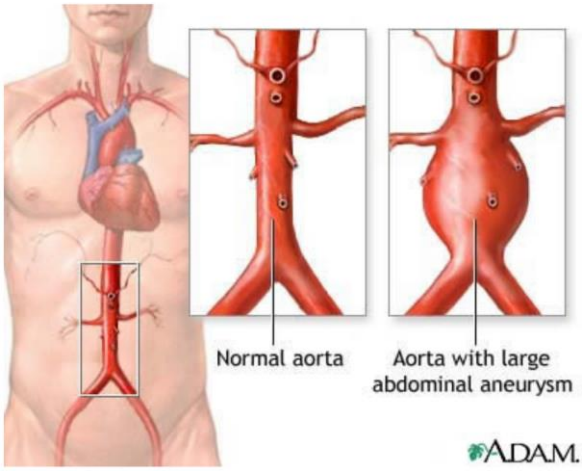

Figure 8 Artistic sketch of AAA in human body. Reprint from[51]**.**

Incidence of AAA in elder population is not negligible; various studies reported AAA prevalence in group of men 65 to 74 years from 1.5% in Sweden[52] to 4.9% in UK[53] and its gradual shift towards higher age [52, 54]. But it is not just older men who are threatened by AAA. Women

form about ¼ of patients with AAA[55]. High age, present or previous smoking and family history of AAA are the major risk factors influencing the incidence of AAA [56].

Typical evolution of AAA includes a first phase of silent growth without symptoms when it does not bring any difficulties to the patient. Typically an AAA grows by some 5mm per year while individual growth rate is in the range $0.18 \div 0.79cm$ per year[50]. Together with its growth the probability of occurrence of AAA rupture also increases. From biomechanical perspective it is in consequence of the LaPlace law saying that stress increases with diameter.

AAA rupture is a life threatening event during which a massive internal bleeding occurs and the overall mortality in this case is about 50% and it does not decrease significantly in the last 20 years[57]. On the other hand, not all AAAs do rupture. Annual probability of rupture is often investigated and represented as a function of its diameter [58–60]; its current estimation is visualized in Figure 9. To complete the image information for a reader, it is important to mention that the 30-days post operational mortality is about 5-8%[58], plus many patients suffer from other diseases simultaneously, so the decision what AAA should be electively (either by open surgery or by endovascular treatment) treated is not at all easy.

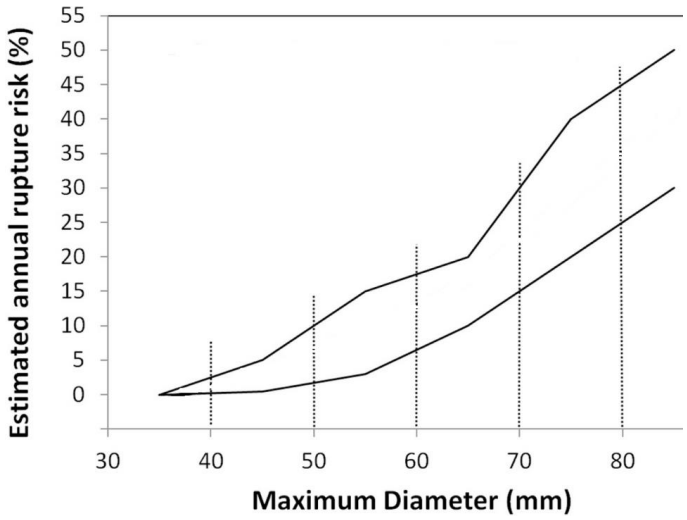

Figure 9 estimated annual risk of rupture for untreated AAAs. Slightly modified from[61]

Despite the complexity of problem the clinical practice found a scheme which works somehow. Nowadays a patient with AAA is suggested for intervention if its maximal diameter exceeds 55mm in men and 50mm in case of women[62], or if the AAA grows by more than 0.5cm in 6 months[50, 62]. This approach is called the maximal diameter criterion.

Unfortunately the criterion of maximal diameter has severe intrinsic limitations. Although AAA larger than 55mm are currently treated, the annual risk of rupture for a 75mm large AAA may be as low as 12% [63] or in other words some 90% of large AAAs would not rupture within the next year and therefore the surgery could be postponed. This would bring benefits to both patients and the public health insurance system due to a lower number of surgeries to be financed. Of course the critical question is "*how to identify the risky AAA?*" This question motivates the whole research of the Author of this thesis.

3.5.1 Pathology of AAA

If you want to recognize the risky AAA you must be already familiar with ongoing pathological changes in the AAA wall. AAA is a disease primarily affecting the aortic media[64], specifically elastin. It has been demonstrated that canine arteries treated by elastase underwent always a significant diameter expansion[65] while their treatment by collagenase led to only minor diameter increase followed by artery rupture[65]. Other studies confirmed the elastin in AAA is degraded and fragmented [5, 66]. Interestingly, it has been also demonstrated that AAA has 4-to 6times more tropoelastin protein compared to healthy aortas[67] which shows there is an intensive but ineffective elastogenesis in the aneurysmal wall[64]. Loss of elastin is demonstrated in biaxial tensile tests of aneurysmal tissue by a significant decrease of the initial stiffness of stress-strain curves[68].

When elastin is absent or is unable to carry the load, the collagen becomes the only relevant load bearing constituent in AAA. Its structure changes dramatically. It becomes much less wavy and significantly more dispersed[69] in directions compared to healthy aorta. This remodeling becomes also evident on biaxial stress-strain curves[68, 70]. The heel region becomes much shorter and the anisotropy decreases significantly as demonstrated in literature[68, 71] and shown in Figure 10. This difference is also evident when Figure 10 is compared with Figure 7.

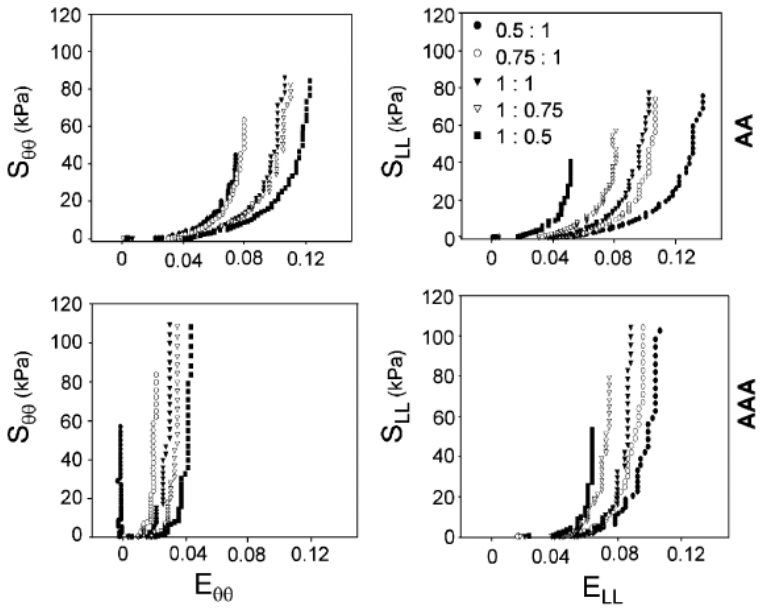

Figure 10 Comparison of biaxial stress-strain curves of normal aorta (upper row) and AAA (lower row). The "heel region" is much shorter, the initial stiffness decreases and anisotropy decreases in aneurysmal tissue. Reprint form [68]

3.5.1.1 Intraluminal thrombus ILT

Besides the already mentioned changes in the aortic wall, the presence of AAA has also other consequence. It results in formation of a new structure inside the AAA. It is called intraluminal thrombus (ILT). ILT is present is vast majority of AAAs and it is thought to develop in order to keep the lumen of the artery roughly with the same diameter as it has outside the AAA to prevent turbulent blood flow inside the AAA. It is basically a blood clot which is attached to the inner surface of the AAA. Its constitution is not clear. Some authors state it is formed mainly of fibrin (the same protein which creates the regular blood clot) which creates a dense mesh of fibers attached from one part of the wall to another one[72] while others consider this to be a temporary state of a fresh ILT and they think fibrin in the ILT is later (in order of years) replaced by collagen fibers[73, 74]. It is noted that this issue is hard to determine; if there are collagen fibers in the ILT they are located in the older ILT which is close to arterial wall and often severely disrupted[75]. Consequently it is not easy to distinguish the boundary between the ILT and aneurysmal wall.

The effect of ILT on aneurysmal wall is also not very clear. It has been shown it prevents transport of oxygen towards the wall[76] which correlates with lower wall strength measured under the ILT[76, 77]. Also it is reported the wall behind ILT is thinner[77] and more affected by

inflammatory response[75, 78]. On the other hand, it has non-negligible mechanical properties (isotropic with Youngs's modulus of about 50kPa[70, 79]) and both numerical[80–82] and experimental[72] studies show consistently that the presence of ILT is associated with a lower deformation and lower wall stress under the ILT than beyond which supports the hypothesis the ILT has also a positive effect since it helps to carry the load of blood pressure. Therefore it is consistently included in numerical simulations of AAA since the year 2000 or so.

3.5.2 Wall stress and AAA

The above described changes are typical for all AAAs and histological analyses state globally there is no difference in aneurysmal wall in the ruptured and intact AAAs[83]. This suggests the AAA rupture relates to some local state of the aneurysmal wall. Many authors believe the key factor is the wall stress in the AAA. They are mostly inspired by the fundamental study of Fillinger et al. [84] which showed for the first time that wall stress can be used to discriminate between intact and ruptured AAAs and, moreover, this wall stress is better than the maximum diameter criterion. This result was confirmed several times since (see [84] and references therein) and the effort has been focused on including all important features which have a significant effect on the wall stress in AAA.

4 Commented list of Author's publications

The author of this thesis dedicated his effort to the task described above both during and after his doctoral study. Due to continuity in his work on this subject there is not a clear splitting line what was done before and after the Author's doctoral defense. Investigation of effect of ILT failure [81] and effect of poroelastic nature of ILT on wall stress in AAA[86] were published before the Author's Ph.D. defense (which was 14.9.2012) while some work on other topics discussed further was done as well. However, papers regarding that were either not prepared or not accepted by the time of the Author's Ph.D. defense and also reviewers often required major changes in the manuscripts which have been done after the Author's Ph.D. defense. This date was therefore used as a splitting line and the manuscripts accepted after the period of the Author's doctoral study are included in chapter 2. Finally, it is noted the first manuscript [A] was accepted four months (20.1.2013) after Author's Ph.D. defense which justifies its inclusion here.

4.1 Summary of citations

Most recent information about Authors scientometric parameters can be found either on ResearcherID.com (which gathers information from Web of Knowledge.com) : http://www.researcherid.com/rid/H-7386-2016, on Researchgate.com: https://www.researchgate.net/profile/Stanislav_Polzer or alternatively on google.scholar.com: https://scholar.google.cz/citations?user=dAHkywMAAAAJ&hl=cs. Overall, this Author has $h-index = 6$ (according to WoK) at the time of this thesis submission. More information about number of citations both globally and specifically for each publication can be found in Table 1.

Publication	No.of citations according to WoK with (without) self-citations	No.of citations according to Scopus with (without) self-citations
All –including papers published before Author's Ph.D. defense	86 (75)	97 (75)
All –excluding papers published before Author's Ph.D. defense	47 (40)	52 (38)

A- Polzer S, Bursa J, Gasser TC, Staffa R, Vlachovsky R. A numerical implementation to predict residual strains from the homogeneous stress hypothesis with application to abdominal aortic aneurysms. Ann Biomed Eng 2013;41:1516–27. doi:10.1007/s10439-013-0749-y.	10 (9)	10 (8)
B- Polzer S, Christian Gasser T, Bursa J, Staffa R, Vlachovsky R, Man V, et al. Importance of material model in wall stress prediction in abdominal aortic aneurysms. Med Eng Phys 2013;35. doi:10.1016/j.medengphy.2013.01.008.	16 (13)	19 (14)
C-Polzer S, Gasser TC, Forsell C, Druckmullerova H, Tichy M, Staffa R, et al. Automatic identification and validation of planar collagen organization in the aorta wall with application to abdominal aortic aneurysm. Microsc Microanal 2013;19. doi:10.1017/S1431927613013251.	7 (6)	8 (4)
D- Polzer S, Gasser TC, Novak K, Man V, Tichy M, Skacel P, et al. Structure-based constitutive model can accurately predict planar biaxial properties of aortic wall tissue. Acta Biomater 2015;14. doi:10.1016/j.actbio.2014.11.043.	9 (7)	10 (7)
E- Polzer S, Gasser TC. Biomechanical rupture risk assessment of abdominal aortic aneurysms based on a novel probabilistic rupture risk index. J R Soc Interface 2015;12. doi:10.1098/rsif.2015.0852.	0 (0)	0 (0)
F- Novak K, Polzer S, Tichy M, Bursa J. Automatic Evaluation of Collagen Fiber Directions from Polarized Light Microscopy Images. Microsc Microanal 2015;21. doi:10.1017/S1431927615000586.	3 (3)	3 (3)
G- Khan S, Verma V, Verma S, Polzer S, Jha S. Assessing the potential risk of rupture of abdominal aortic aneurysms. Clin Radiol 2015;70:11–20. doi:10.1016/j.crad.2014.09.016.	2 (2)	2 (2)
H- Slazansky M, Polzer S, Man V, Bursa J. Analysis of Accuracy of Biaxial Tests Based on their Computational Simulations. Strain 2016;52. doi:10.1111/str.12205.	0(0)	(0)

Table 1 Citation information

4.2 A numerical implementation to predict residual strains from the homogeneous stress hypothesis with application to abdominal aortic aneurysms

4.2.1 Commentary to the paper

Motivation for this paper came from the Author's previous work [81, 86] as well as from investigation of other studies [87, 88] where wall stress in real AAAs was computed. All of these studies showed remarkable stress gradients across the aneurysmal wall especially in areas of peak wall stress which is used as a decisive quantity for discrimination between safe and risky AAAs [85, 87–89]. This was consistent in all patient-specific studies at that time and also with direct contradiction to the widely accepted uniform stress theory[90]. This theory states the arterial wall is constantly remodeled by cells in its structure in order to achieve their uniform loading across the thickness. This remodeling results in residual strains which are consistently observed in arteries [28, 90, 91]; they demonstrate themselves by opening of an axially cut ring of the artery. This opening can be quantified by so called opening angle parameter and many studies incorporate residual stresses (RS) by creating this opened geometry and then numerically closing it[92, 93]. Bending generated during the closing generates negative stresses at the inner surface and positive at the outer surface. If the geometry is then loaded by a blood pressure, the combination of RS with the stresses induced by the blood pressure results in a homogeneous stress distribution across the thickness. However, this approach has two major limitations.

First, it requires knowledge of the opened geometry which is of course unknown when an in-vivo AAA is analyzed. And even if one could somehow generate this opened state artificially, another problem concerns numerical difficulties associated with large deformation FEA; therefore this approach is limited to small arteries (where the deformations associated with reaching the opened geometry is relatively small too) or idealized geometries[93, 94]. In contrast to this approach we proposed a different method which is based on decomposition of deformation gradient tensor into elastic and growth parts. The isotropic volumetric growth was iteratively adjusted in order to achieve the desired vanishing of stress differences between the outer and inner surfaces. The advantage of this approach is in the fact that one does not need to know the RS distribution a priori but the RS are induced as a direct consequence of fulfilling the homogeneous stress hypothesis. Moreover, we demonstrated this approach is applicable to general geometries such as

AAA. Another less obvious advantage is in the fact that the computed maximum wall stresses are much lower compared to the case without RS and we believe they are also more realistic. Their insensivity to mesh density can be also achieved with a much coarser mesh as shown in Figure 11 which partially eliminates the disadvantage of longer computational time given by iterative nature of our algorithm. Finally, it is noted our algorithm results in more homogenous stress distribution not just across the wall but also over the AAA surface which should be also approximately homogenous according to the uniform stress theory although validity of this on AAA volume was not proven yet and the Author believes it is reasonable to expect some disturbance of it due to the pathological nature of AAA.

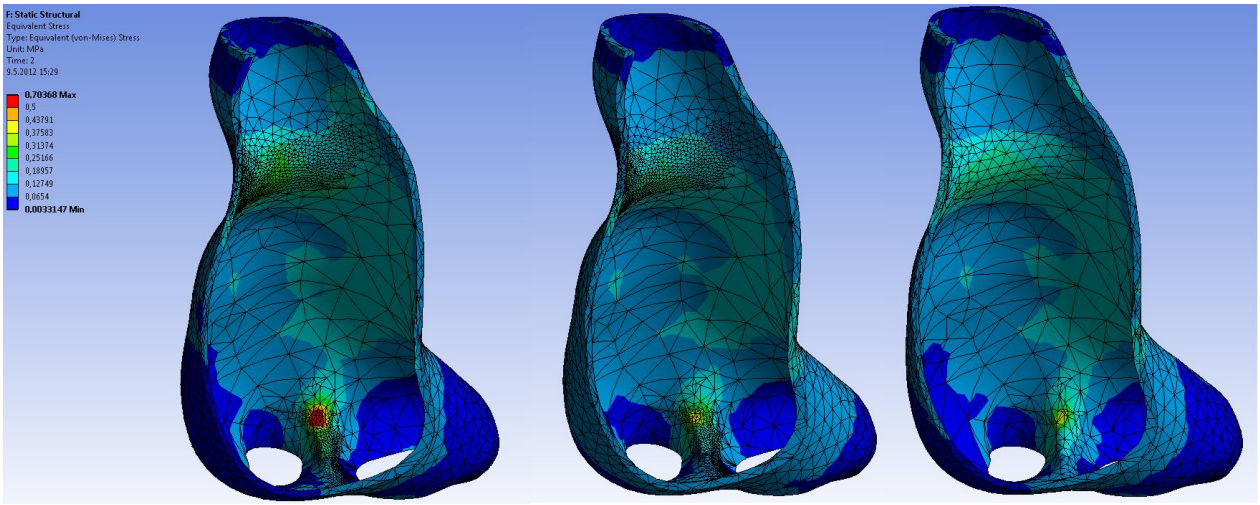

Figure 11 Demonstration of the effect of RS and mesh density on stress distribution in typical AAA. Von Mises stress distribution when RS is omitted (left) leads to higher stresses for which a locally fine mesh needs to be used. When RS algorithm is applied (middle) the stresses are much lower and much more uniform not only across the wall but also over the AAA. Finally, it is shown that the same stress distribution with RS can be obtained with 3x larger elements (right).

4.2.2 Fulltext

Starting on a next page.

4.3 Importance of material model in wall stress prediction in abdominal aortic aneurysms

4.3.1 Commentary to the paper

Since the 2006 there is one major contradiction in the available experimental data regarding mechanical response of aneurysmal tissue. The most relevant paper published till 2006 was by Raghavan et al.[71] where uniaxial tensile tests of aneurysmal samples were performed. Later this experimental data were nicely fitted by an isotropic constitutive model[95] which became one of the most cited papers in this field ever. Nevertheless, the same group published in 2006 experimental biaxial tensile tests of aneurysmal tissue which were completely different[68] from the previous data as shown in Figure 12. Such differences cannot be explained by different substance of the performed tests (biaxial response should be always stiffer than uniaxial) and reasons for that discrepancy remain unclear till now. Studying those papers, however, brought the Author of this thesis to the following question: ”How sensitive are the wall stresses in AAA to the material model applied?”

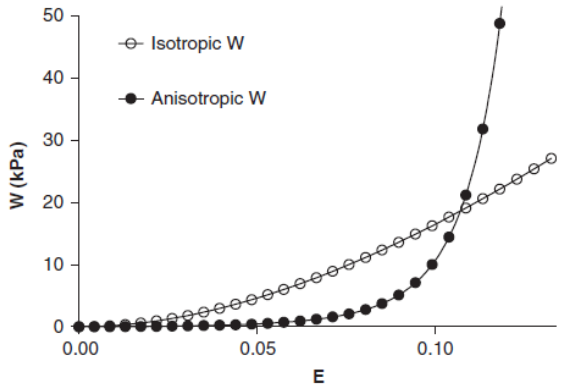

Figure 12 SEDF for uniaxial (noted as isotropic) and biaxial (noted as anisotropic) data. Reprint from [68]. Uniaxial response is initially much stiffer and its stiffness increase only moderately with deformation while biaxial response is initially much more compliant but stiffens dramatically at certain strain values.

To answer this question, the Author of this thesis performed FEA of 7 patient specific geometries of AAA using various material models. In this paper we used both models described above and, morover, one even stiffer[96] and one patient-specific model which was obtained by our own biaxial testing of aneurysmal tissue of the analyzed AAAs. This testing confirmed the biaxial response of AAA tissue is similar to that measured biaxially by vande Geest et al.[68]

Further, it was necessary to remove the effect of the deformed geometry. Naturally, a stiffer material model would lead to smaller deformations compared to a more compliant one, and it is known that stresses are a direct consequence of the deformed geometry. Therefore it was required to ensure the deformed geometries to be the same irrespective of the material model applied. This is a problem of inverse elastostatics when the deformed geometry is known together with load which caused it and the unloaded configuration is to be determined[97]. This problem was already solved for AAAs before so we only adopted the available algorithm[98].

Once the stresses had been computed, the Author of this thesis performed also their comparison. Here it is underlined we did not limit ourselves to comparison of peak wall stress only but, for the first time in the world literature, we also compared the whole stress fields. This was possible because for all materials we used the same mesh and, consequently, we knew stress values in the same points. So for each node we subtracted the von Mises stress obtained for the patient specific material model (which served as etalon here) from the stresses obtained for other models. Then we made histograms of these differences. Here a narrow distribution around 0kPa means the stresses are mostly identical with the patient specific model for the chosen material model. while, on the contrary, a wide flat distribution or its peak shifted away from the 0kPa difference show a significantly different field. This was a key step which revealed significant differences between individual material models because simple comparison of peak wall stresses did not bring any clear conclusions.

Finally, we demonstrated the matters of the material models by showing stress distributions on an ideal tube and we clearly showed that the stresses on both surfaces differed greatly from each other when an initially compliant material model was used. Contrary, a stiff material model yielded in very similar stresses on the outer and inner surfaces as stated by the Laplace law. The only major limitation of this paper was that we neglected RS because, at that time, we did not published yet the paper [A] so we could not reference to it. Investigation of the effect of material model when RS is respected is one of the ongoing research topics of the Author of this thesis.

4.3.2 Fulltext

Starting on the next page.

4.4 Automatic identification and validation of planar collagen organization in the aorta wall with application to abdominal aortic aneurysm

4.4.1 Commentary to the paper

This research was mainly motivated by feedback provided to the Author by reviewers of his papers. They consistently pointed out the fact that aneurysmal tissue is also anisotropic (see chapter 3.5.1 and [68, 70]) so the Author's approach using isotropic constitutive models [**A, B, E**, 81, 86] is simplification which can be overcome. Therefore the Author of this thesis started to investigate the possibility to include an anisotropic constitutive model into his computational model. However, immediately it was found out that there was simply not enough information for that. Most importantly, the information about local orientation of principal material axes is missing; it represents a necessary input if anisotropic model is to be employed. Since it is also known that the anisotropy arises from the collagen distribution (see chapter 3.1.2) it was logical to focus on collagen structure. Surprisingly, most information about collagen structure in arterial wall at that time came from manual measurements of collagen orientation using polarized light microscopy and Picrosirius red staining[21, 23]. The weak point of those studies was very low number of measurements per image (usually less than 30) which could of course hardly provide any relevant information about dispersion of fiber directions. Although there were also some automated algorithms [19, 22, 26, 99, 100], out of which the fast Fourier transform (FFT) based algorithms were the most promising. The reason is they are applicable to virtually any image and they are not computationally expensive which allows you to analyze large number of images. The weak point of all FFT based algorithms was in their qualitative nature; in other words, they were not capable to quantify the dispersion of fiber directions[100–102].

This paper was therefore focused on developing an automated algorithm to estimate mean fiber orientation as well as its dispersion. At first we have shown the sensitivity of FFT based algorithms to intensity of visual display of fibers and its noise to proof that a raw (unadjusted) histogram obtained from the FFT spectrum cannot provide quantitative information about fiber dispersion. With the same set of artificial images we have also demonstrated the key feature of our new algorithm which is its powering and consequent normalizing done with the aim to ensure its integral equals one again. It was also shown that a properly powered histogram offers a quantitative information about fiber dispersion.

Unfortunately it also means that our algorithm must be calibrated to the analyzed tissue at the beginning. We perform this calibration on 10 samples of aneurysmal tissue where the histogram obtained from analyzing one image with the powering was compared (by calculating R^2) with the histogram obtained from 625 manual measurements of sub-images covering the same area. Results showed a strong correlation between concentration parameter b and R^2 which means that our method is reliable when $b > 1$. In other words, we can reliably estimate fiber dispersion if the fibers have some preferential direction. Here it is noted $b = 0$ means isotropic fiber distribution while $b > 20$ means practically unidirectional distribution of fibers. A relevant part of this analysis is our conclusion that the proposed method is reliable in those ranges where the material stiffness in the stiffest direction is by at least 50% higher compared to the stiffness in the most compliant direction. Nevertheless, the unreliability of our method for largely dispersed fibers is not a severe limitation because such material behaves more or less isotropically thus the information about principal material directions is not important

Another interesting result of this study came from comparison with polarized light images where we found out that the proper powering value is different compared to the sub-image analysis which means our algorithm must be calibrated for each tissue and staining method. Although it is admitted such a calibration takes about a week, once it is done the analysis of one image is a matter of seconds which makes this method an ideal candidate for analyses of large sets of images as the Author performed in another study [**D**] described in chapter 4.5.

4.4.2 Fulltext

Starting on the next page.

4.5 Structure-based constitutive model can accurately predict planar biaxial properties of aortic wall tissue

4.5.1 Commentary to the paper

Author's original motivation for this study is related to study [**C**] where a new automated method for estimation of collagen fiber directions was proposed. Naturally, as a next step, the Author wanted to apply this method on an easily accessible tissue of porcine aortas to confirm the often mentioned observation of two families of fibers present in arterial wall as described in chapter 3.1.2. Therefore we used 9 samples of porcine aorta 18x18mm large and cut them in a 120μm span in the radial direction across the whole thickness. The samples were then stained by Picrosirius red to enhance the collagen visibility and analyzed using the method described in chapter 4.4 and study [**C**]. Overall some 9000 images were captured and analyzed which makes this study by far the most detailed one in this field.

Surprisingly, the results have not confirmed the existence of two families of fibers, but existence of only one preferential fiber direction was observed instead. Moreover, we found a gradual change in fiber dispersion as shown in Figure 3 in study [**D**] (Full text in chapter 4.5.2). The inner media showed the most unidirectional structure of collagen fibers while the dispersion gradually increased and adventitia showed almost isotropic fiber orientation. Such a structure was not described before. According to Author's opinion it is because previous studies analyzed by orders lower numbers of measurements[8, 9, 21, 22]. We also observed two families of fibers in individual images but this phenomenon vanished when images from the whole histological slice were considered together.

The above described controversial observation was also validated in the second part of the study where we tried to fit, as well as to predict biaxial behavior of porcine aortic tissue. We used two layered Martufi-Gasser material model (constitutive equation for one layer corresponds to eq.(7)) which contains parameters of mean fiber orientation and its dispersion around this orientation. So we used the above described structural observation in constraining those parameters. The parameters related to collagen waviness were fixed according to values reported in the literature so the only free parameters were those related to the stiffness of either collagen or elastin. This model was able to capture accurately planar biaxial tensile tests of 18 samples of porcine aorta. However, this observation is not so important as the fact it was also capable to predict accurately

(median of $R^2 = 0.88$) other loading protocols when fit to only one biaxial protocol (best results were obtained for the protocol with circumferential to axial displacement ratio of 2:1). Such accuracy in a constitutive model prediction was achieved for the first time. This result is especially important because other known models have severe problems to predict any loading regimes different from those they were fitted on. Practical consequence is in a reduced reliability of computational simulations when they are used to model material response outside the space the material model was calibrated on. Our result shows for the first time that a proper structure-based constitutive model can overcome this limitation. Therefore the Author considers this constitutive model as an ideal candidate for his computational model in rupture risk assessment of AAA.

Impact of this result is further increased by the fact we used by far the largest stress ranges in testing. While other studies tested specimens to some 150kPa [23, 68, 70], we were able to stretch the samples up to 420kPa without tearing it. This is consequence of the setup of our biaxial machine which uses clamps instead of hooks; both these ways of specimen gripping are further analyzed in chapter 4.9 and paper [**H**].

4.5.2 Fulltext

Starting on the next page.

4.6 Biomechanical rupture risk assessment of abdominal aortic aneurysms based on a novel probabilistic rupture risk index

4.6.1 Commentary to the paper

The entire Author's previous effort headed towards a proposal of a new concept how to estimate the rupture risk index for an AAA. The main motivation raised from an analysis of available literature where all of the published concepts are deterministic [85, 87, 88]. It means the rupture risk is usually estimated from the value of PWS [84, 89, 103] which is calculated for somehow chosen (but still deterministic) values of wall thickness, blood pressure, mechanical properties of both aneurysmal wall and ILT, etc. Another option is that rupture risk is calculated from the ratio of wall stress to local wall strength which is called the peak wall rupture index (PWRI) [87] or rupture potential index [104]. Wall strength is usually predicted on the basis of the study by vande Geest et al.[105] where correlations between wall strength and other patient specific parameters (which can be estimated in vivo - such as sex, blood pressure, ILT thickness, etc.) were assessed and an equation for predicting patient-specific local wall strength was proposed. Nevertheless, all of these approaches neglect the uncertainty which inevitably exists in most of those parameters. Therefore the Author has proposed a new approach taking the uncertainty in wall thickness and wall strength into consideration as the first step. The wall thickness was included because it is currently impossible to detect it from standard CT-A images.

First, the Author integrated his previous studies [**A, B**] into his computational model to estimate patient specific PWS. This model is currently the most advanced according to the best Author's knowledge. It respects both unloaded geometry of AAA as well as RS which was not done before on patient-specific AAA geometries. Also the used FE mesh is the most advanced in the field because the Author was able to generate purely hexahedral mesh on general patient-specific geometries of aneurysmal wall as also demonstrated in Figure 13. On the other hand, the mesh for ILT was still generated as a free mesh with linear tetrahedrons due its irregular geometry as shown in Figure 14. ILT was usually meshed with a fine mesh to overcome volume locking phenomena known for linear tetrahedrons. Despite this, the ILT mesh can be considered as a limitation of used model because it is not so fine to ensure full mesh independence of the results and the Author performed already some additional analyses revealing the proper element size

would have to be about 1mm. However such a mesh would be too large to be solved on current computers.

The chosen constitutive model is an isotropic approximation of the published biaxial response of AAA[68]. Here it is admitted some other studies already employed anisotropic constitutive models for aneurysmal wall [106, 107] and the Author is working on gaining all the necessary information to be capable to employ an anisotropic constitutive model reliably and to analyze its impact on the computed stresses (see chapter 4.5).

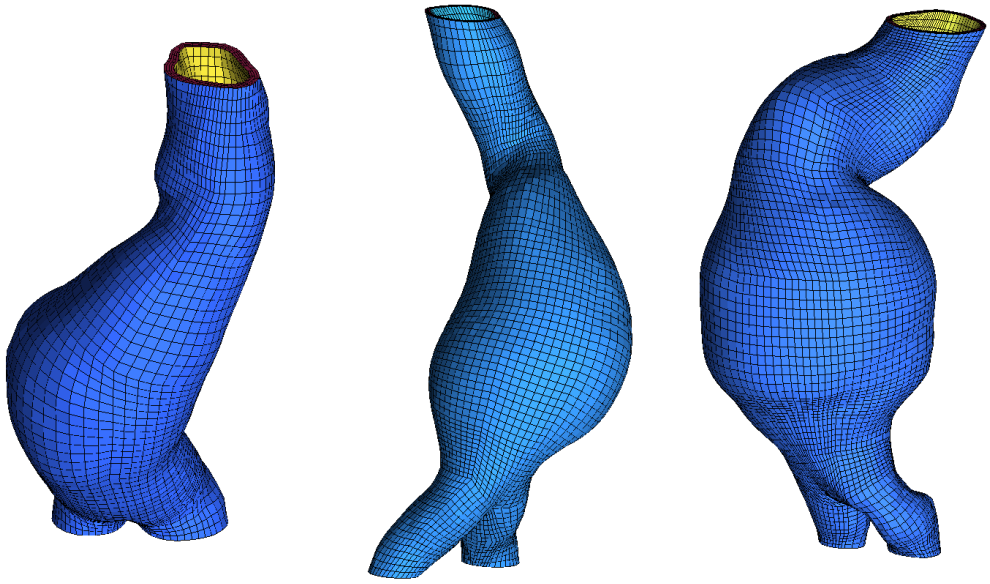

Figure 13 FE mesh for three representative patient specific AAAs confirming it is possible to obtain pure hexahedral mesh even for very irregular geometries

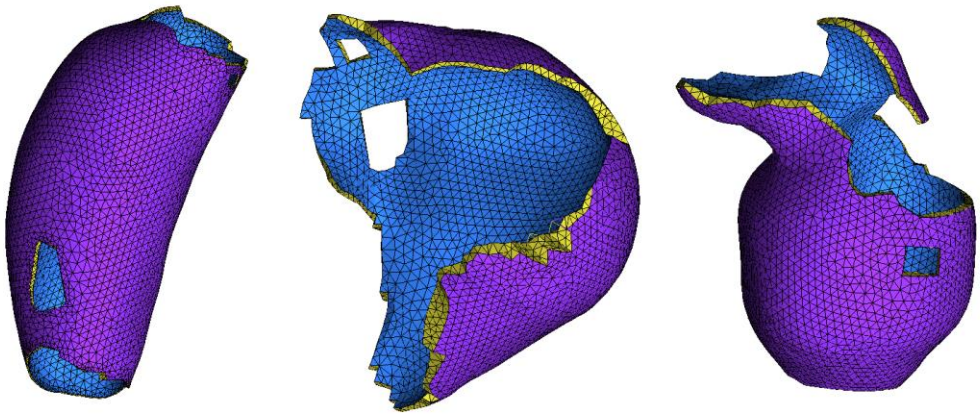

Figure 14 Typical FE meshes of 3 chosen patient specific ILTs. ILTs are meshed by a free mesh due to highly irregular geometries

However, the main novelty of this paper is in the analysis of the computed PWS. For each geometry the Author generated 3 FE meshes with different wall thickness. Then the computations of PWS were performed three times for different wall thicknesses. Finally, we fitted an inverse power law function $PWS = a \cdot h^{-m}$ to obtain an analytical expression of the dependence between the calculated PWS and wall thickness. This analytical expression was then used in Monte Carlo simulations where PWS was repeatedly ($10^6 times$) computed for various wall thicknesses which followed a known distribution[77]. By using this approach a statistical distribution of PWS as a consequence of wall thickness distribution was obtained. The second important step was to take the distribution of wall strength into account. We used the data published before[77] and fitted a distribution function to it. So now we had two distributions, the former for PWS and the latter for wall strength, and we had to compute the probability that PWS will be lower than the wall strength which would cause the rupture. If the PWS is deterministic then it is simply an area below the strength distribution integrated up to PWS as shown in Figure 2 in the paper full text. For the case that PWS has also some distribution, the more general eq. 2.7 (in the full text) is to be used. This probability of rupture was entitled probabilistic rupture risk index (PRRI) in this paper.

PRRI has a few remarkable differences compared to the deterministic PWRI. First of all, it has clear boundaries. It cannot be lower than 0 and higher than 1. This gives a user an idea how to assess the obtained values. On the contrary, the PWRI does not have an upper boundary so it is difficult for the surgeon to assess the true risk of patient with a given PWRI. Second, difference in the PRRI is highly nonlinear; it rises very slowly with increasing mean PWS value up to a certain point when PRRI becomes very sensitive to PWS and a change in PWS of 5% may result in a 5times increase of PRRI. On the other hand, for very high PWS the PRRI becomes insensitive again which makes sense because if PWS is 2 times or 4 times above the mean strength the change in PRRI is very small (from 97% to 99% or so). In both cases the PRRI illustrates clearly the risk of the given AAA.

The proposed method has been validated on a small cohort of 7 intact and 7 ruptured AAAs and it showed a better discriminative capability than any other known method.

4.6.2 Full text

Starting on the next page.

4.7 Automatic Evaluation of Collagen Fiber Directions from Polarized Light Microscopy Images

4.7.1 Commentary to the paper

When the Author of this thesis had published paper [**C**] (see also chapter 4.4) he noticed limitations of the algorithm presented there. Most of all, the FFT based method needs calibration before use. In [**C**] this was done by manual capturing of a great set of images of the chosen area (typically about 500 images per sample; 3-5 samples used for calibration [**D**]). This is a very time consuming process. Another limitation is in generality of the FFT based algorithm. It cannot distinguish between individual structures (it only prefers more contrast structures [**C**]) while in the field of arterial biomechanics we are often interested only in the orientation of collagen fibers[21, 22, 69, 101]. On the other hand, polarized light microscopy (PLM) is collagen specific, so data from PLM could be used to calibrate our FFT-based algorithm. However, estimation of collagen fiber orientation from PLM images was at that time mainly manual [22, 69] with very low numbers of the measured orientations per image. Therefore the Author decided to develop an automated algorithm to estimate collagen fiber orientation (including dispersion) automatically.

Estimation of local collagen fiber orientation is simple. Human operator chooses a bright point in the histological slice enlightened by polarized light and rotates with the slice until this point extinct (becomes completely dark, its intensity=0). Now the collagen fiber orientation is perpendicular to the direction of the polarizer. As its orientation is known the operator thus knows also the fiber orientation in the chosen point. The Author proposed an algorithm which was able to replace the human operator.

First it was necessary to obtain a set of mutually rotated images. Then we applied phase correlation algorithm to align those images. Consequently we were able to track the evolution of intensity during the rotation of the slice. We found out that 3 images are sufficient for this analysis so for each point we obtained three values of its intensities as a function of angle. Finally, a very simple sinus-like function with periodicity of 90° was fitted to this three points and the angle of its minimum was estimated because it should coincident with the angle of fibers in the given point as estimated by human operator.

The proposed algorithm was validated on 12 images of two different tissues against two human operators. Results showed that human operator may tended to underestimation of the measured orientation which can be explained by limited human eye sensitivity. For human eye the given point appeared dark at large range of angles (about 15°) and usually human operator has not found the darkest point orientation accurately. The results were also tissue dependent; a much better agreement was obtained when Achilles tendon tissue was analyzed (about -0.6°) compared to porcine aortic media tissue (-6.7°).

Naturally, the proposed algorithm is capable to analyze by several orders higher number of points compared to human operators. In our case it was about 35k points per each aortic tissue sample . For comparison, those studies where manual measurements were performed analyzed about 30-50 points per sample[23, 69]. Such increase in the number of analyzed points allows us to get much more detailed information about structure of the analyzed image and provides thus comprehensive information about fiber dispersion which is necessary for calibration of our previously published FFT-based algorithm [**C**].

Another interesting result came from the analysis of artificial wavy fibers which produced histograms with two distinct peaks (see Figure 6 in the full text). This brings us to another potential explanation of differences between collagen distribution observed by the Author o [D] and other authors who observed two families of fibers [8, 9, 21, 22] when analyzing the structure of arterial wall by PLM. It is very well possible that those authors observed wavy fibers heading globally in the circumferential direction as it was captured by our FFT algorithm [**D**] while they observed local orientations of fibers which are mostly symmetrically declined from circumferential direction due to their waviness. Nevertheless this hypothesis is waiting for its validation and requires an approach capable to distinguish between local and global directions of fibers.

Finally, it is noted that the Author came with the idea and an initial version of the script while Ing. Novák (for whom the Author is supervisor specialist of his doctoral topic) continued on improving the script and validated it.

4.7.2 Full text

Starting on the next page.

4.8 Assessing the potential risk of rupture of abdominal aortic aneurysms

4.8.1 Commentary to the paper

Author of this thesis was asked by Dr. Khan from Pittsburgh University to cooperate on his prepared review regarding rupture risk assessment of AAAs. This review was intended to be accessed primary by vascular surgeons and radiologists. This fact influenced the choice of information provided there.

In the introduction the AAA is defined, and explanation of 5.5cm AAA size as a threshold for intervention is provided. It is also explained how the size of AAA is usually measured and differences between individual ways of measurements are discussed pointing out that estimation of AAA size is not a trivial and closed problem at all. For screening purposes the ultrasound measurement should be preferred while the actual size should be also confirmed by CT angiography since it is less operator sensitive. On the other hand various diameters can be estimated from CT scans (for instance maximal diameter in axial slice, minimal diameter in axial slice, maximal anteroposterior diameter or maximal orthogonal diameter) and they can vary significantly and affect thus the timing of intervention.

Next chapter is dedicated to discussing epidemiological factors associated with the risk of AAA rupture such as female gender[108] with underlining the risk of rupture is four times higher for female patients. Then smoking (through increase of elastin degradation), hypertension (which increases load of the aneurysmal wall) and family history (which probably affects the structure of aneurysmal wall and also speed of elastin degradation and/or collagen production) are mentioned as the most important risk factors for AAA rupture. Speed of AAA growth is further discussed and its association with probability of AAA rupture is shown.

Majority of Author's work on this paper was in the chapter where biomechanics of AAA is explained. First it was necessary to explain differences between various stresses in AAA (hoop, axial, shear) and their impact on the risk of rupture, as well as to give the reader an idea of their magnitudes. Then several studies have been referenced where PWS or rupture potential index were suggested as an alternative rupture risk predictor, and they were discussed with emphasis on their clinical applicability.

4.8.2 Full text

Starting on the next page.

4.9 Analysis of Accuracy of Biaxial Tests Based on their Computational Simulations

4.9.1 Commentary to the paper

Main motivation for this work came from reviews of the Author's previous papers [**B, D**] where the reviewers pointed out that the gripping method used by our team in biaxial tests of arterial tissue was not validated. They were concerned that use of clamps instead of hooks might lead to inducing stress concentrations in the central part of the specimen where measurement was performed, or the clamp might constrain deformation of the surrounding tissue which would again affect the accuracy of our method. That is why we decided to analyze this problem thoroughly.

We performed a multiparametric computational study where we have analyzed impact of the gripping method ($2 \div 5$ hooks and 2 clamps), size of gripping element, specimen size, testing protocol and type of the tested material on accuracy of the performed experiments. Here the accuracy was assessed by means of computed R^2 value characterizing accordance between the known stress-strain curves of a given material and the estimated stress-strain curves. Construction of the estimated stress-strain curves was identical as we did it during our experimental testing so thus forces were recorded at the ends of hooks or clamps, average strain was calculated from four dots made in a central part of the model etc. The advantage of numerical simulation was that we knew exactly the stress-strain behavior of the tested material since this is an input for FEA. Also the used method of accuracy estimation was novel because other studies have usually analyzed homogeneity of strain field in the sample only [109, 110] while we provide an answer to the question how accurately have we captured the mechanical behavior of this known material.

The numerical model used in this study was as more advanced one compared with other studies[109, 110]. We performed analyses in 3D which allowed us to include effects such as squeezing of material by clamps or uneven strain distribution across the thickness. Also we modeled whole the leverage system and not just gripping elements as usual in other studies. Consequently the force distribution in individual griping elements was not a direct input of the analysis but consequence of static equilibrium. We also analyzed various material types, isotropic and anisotropic, stiff and compliant, progressively stiffening and softening. This was motivated by the known large variability of mechanical properties of soft biological tissues.

Numerical results confirmed that two narrow clamps had a comparable accuracy compared to gripping via hooks. Increase of clamp width led initially to higher accuracy because a wide portion of material was stretched while use of too wide clamps (above 3.5mm) resulted in a decreased accuracy which was caused by constraining the perpendicular deformation under the clamps. Consequently clamps should have a proper size from 2 to 3 mm to achieve the highest accuracy. This observation was consistent for all materials. In the case of hook size the results suggest the larger hooks should be used when 2 hooks per side are used while for 4 or 5 hooks per side the accuracy was the highest for the thinnest hooks.

The interesting conclusion made from this parametric study underlines the importance of a homogenous force distribution across the sample. We have shown that use of high number of gripping elements per side inevitably results in uneven force distribution because even distribution is prevented by the perpendicular elements in the sample corner. This has not been stated explicitly before and several studies preferred as many hooks per side as possible [111, 112].

Besides the numerical study, we also validated our results experimentally. We have tested 10 specimens of porcine aorta using different ways of gripping and fitted the chosen constitutive model to the obtained curves. To reveal any dependence of the results on the order of testing, 5 samples were tested first using a two clamps gripping system and then using a 4 hooks setup, while another set of 5 samples was tested vice versa. This testing and fitting revealed a statistically significant but practically very small difference in the achievable quality of fit ($R^2_{hooks} = 0.984\ vs.\ R^2_{clamps} = 0.9797\ \ p = 0.0043$). Finally, we also tested the maximal stresses which can be induced by both gripping methods in the tested samples before failure under equibiaxial loading conditions (5 samples per method). This experiment proved clamps are able to stretch the samples to higher stresses compared to the 4 hooks system. This difference is caused by a higher stress concentration induced by individual hooks which literally tears the material while the clamps only squeeze it at a larger area. It means clamps can be used to test samples in a wider range of stresses as we have already shown previously [**D**].

4.9.2 Full text

Starting on the next page.

5 Conclusion

In this thesis Author showed overview of his scientific research since his Ph.D. defense. All of his work was motivated by an effort to provide a reliable computational model to assess rupture risk of AAA. Reliable identification of risky AAAs has been one of critical issues of arterial biomechanics recently. The Author has solved several partial problems on this track, from incorporating RS into patient specific models of AAA [**A**], underlining of the importance of material model on wall stresses in the AAA [**B**], up to the proposal of new stochastically motivated probabilistic rupture risk index of AAA [**E**]. Some joint problems have been addressed as well, such as automated measurement methods of collagen orientation in arterial wall [**C**, **F**], demonstration of advantages of using clamps instead of hooks during biaxial tests [**H**] or identification of a robust constitutive model which can reliably predict biaxial behavior of arterial wall [**D**]. As a side effect the Author also provided new information about collagen arrangement in the aortic wall [**D**]. Finally, he also contributed to a review aiming at providing research state of art in this area to audience of vascular surgeons and radiologists [**G**].

It is Authors hope he can complete his research in next years by proving the superiority of his approach on a prospective blinded study which would open the door for a wide clinical application of this approach.

6 List of abbreviations and symbols

Name	Abbreviation or symbol	units
Abdominal aortic aneurysm	AAA	N/A
Strain energy density function	SEDF	N/A
Strain energy density function	Ψ	Pa
First invariant of Right Cauchy-Green deformation tensor	I_1	[-]
Waviness	w	[-]
True length of the fiber	L	[m]
Straight distance between fiber's end points	L_o	[m]
Smooth muscle cell	SMC	N/A
Green-Lagrange strain tensor	**E**	N/A
Holzapfel Gasser Ogden	HGO	N/A
Cauchy-Green deformation tensor	**C**	[-]
(Pseudo)invariants of right Cauchy-Green deformation tensor	I_{4i}	[-]
Angle between a fiber family and the circumferential direction	φ	[rad]
Generalized structure tensor	**H**	N/A
Dispersion of fibers	ρ	[-]
Stretch	λ_i	[-]
Pulse wave velocity	PWV	[m/s]
Arterial thickness	h	[m]
Arterial diameter	d_a	[m]
Mass density of the blood	ρ_b	[kg$\cdot m^{-3}$]
Young's modulus	E	[Pa]
Clinical Stiffness of artery	β	[-]
Systolic pressure	p_{syst}	[Pa]
Diastolic pressure	p_{diast}	[Pa]

Arterial diameter under systolic pressure	D_{syst}	[m]
Arterial diameter under diastolic pressure	D_{diast}	[m]
Intraluminal thrombus	ILT	N/A
Residual stresses	RS	N/A
Fast Fourier transform	FFT	N/A
Coefficient of determination	R^2	[-]
Concentration parameter (of fiber directions)	b	[-]
Peak wall stress	PWS	
Peak wall rupture index	PWRI	[-]
Probabilistic rupture risk index	PRRI	[-]
Polarized light microscopy	PLM	N/A
Computed tomography	CT	N/A
Finite element analysis	FEA	N/A

7 References:

7.1 Other References

1. O'Connell MK, Murthy S, Phan S, Xu C, Buchanan JA, Spilker R, Dalman RL, Zarins CK, Denk W, Taylor CA (2008) The three-dimensional micro- and nanostructure of the aortic medial lamellar unit measured using 3D confocal and electron microscopy imaging. Matrix Biol 27:171–181

2. WOLINSKY H (1970) Response of the Rat Aortic Media to Hypertension. Circ. Res. 26:

3. Humphrey JD, Holzapfel GA (2012) Mechanics, mechanobiology, and modeling of human abdominal aorta and aneurysms. J Biomech 45:805–814

4. Arribas SM, Hinek A, González MC (2006) Elastic fibres and vascular structure in hypertension. Pharmacol Ther 111:771–791

5. He CM, Roach MR (1994) The composition and mechanical properties of abdominal aortic aneurysms. J Vasc Surg 20:6–13

6. Gundiah N, B Ratcliffe M, A Pruitt L (2007) Determination of strain energy function for arterial elastin: Experiments using histology and mechanical tests. J Biomech 40:586–594

7. Gundiah N, Ratcliffe MB, Pruitt LA (2009) The biomechanics of arterial elastin. J Mech Behav Biomed Mater 2:288–296

8. Holzapfel GA, Gasser TC, Ogden RW (2000) A new constitutive framework for arterial wall mechanics and a comparative study of material models. J Elast 61:1–48

9. Gasser TC, Ogden RW, Holzapfel GA (2006) Hyperelastic modelling of arterial layers with distributed collagen fibre orientations. J R Soc Interface 3:15–35

10. Martufi G, Gasser TC (2011) A constitutive model for vascular tissue that integrates fibril, fiber and continuum levels with application to the isotropic and passive properties of the infrarenal aorta. J Biomech 44:2544–2550

11. Fratzl P (ed) (2008) Collagen: Structure and Mechanics. Springer

12. Orgel JPRO, Irving TC, Miller A, Wess TJ (2006) Microfibrillar structure of type I collagen in situ. Proc Natl Acad Sci U S A 103:9001–5

13. Andriotis OG, Chang SW, Vanleene M, Howarth PH, Davies DE, Shefelbine SJ, Buehler MJ, Thurner PJ (2015) Structure–mechanics relationships of collagen fibrils in the osteogenesis imperfecta mouse model. J. R. Soc. Interface 12:

14. Carlisle CR, Coulais C, Guthold M (2010) The mechanical stress-strain properties of single electrospun collagen type I nanofibers. Acta Biomater 6:2997–3003

15. Nissen R, Cardinale GJ, Udenfriendt S (1978) Increased turnover of arterial collagen in hypertensive rats (hydroxyproline). Med Sci 75:451–453

16. WOLINSKY H, GLAGOV S (1964) Structural Basis for the Static Mechanical Properties of the Aortic

Media. Circ. Res. 14:

17. Sokolis DP (2008) Passive mechanical properties and constitutive modeling of blood vessels in relation to microstructure. Med Biol Eng Comput 46:1187–1199

18. Roy S, Boss C, Rezakhaniha R, Stergiopulos N (2010) Experimental characterization of the distribution of collagen fiber recruitment. J Biorheol 24:84–93

19. Tsamis A, Phillippi JA, Koch RG, Pasta S, D'Amore A, Watkins SC, Wagner WR, Gleason TG, Vorp DA (2013) Fiber micro-architecture in the longitudinal-radial and circumferential-radial planes of ascending thoracic aortic aneurysm media. J Biomech 46:2787–2794

20. Hill MR, Duan X, Gibson GA, Watkins S, Robertson AM (2012) A theoretical and non-destructive experimental approach for direct inclusion of measured collagen orientation and recruitment into mechanical models of the artery wall. J Biomech 45:762–771

21. Finlay HM, Whittaker P, Canham PB (1998) Collagen organization in the branching region of human brain arteries. Stroke 29:1595–601

22. Schriefl AJ, Reinisch AJ, Sankaran S, Pierce DM, Holzapfel GA (2012) Quantitative assessment of collagen fibre orientations from two-dimensional images of soft biological tissues. J R Soc Interface 9:3081–93

23. Schriefl AJ, Zeindlinger G, Pierce DM, Regitnig P, Holzapfel G a (2012) Determination of the layer-specific distributed collagen fibre orientations in human thoracic and abdominal aortas and common iliac arteries. J R Soc Interface 9:1275–1286

24. Humphrey JD, Dufresne ER, Schwartz MA (2014) Mechanotransduction and extracellular matrix homeostasis. Nat Rev Mol Cell Biol 15:802–812

25. Armentano RL, Barra JG, Levenson J, Simon A, Pichel RH (1995) Arterial Wall Mechanics in Conscious Dogs. Circ. Res. 76:

26. Timmins LH, Wu Q, Yeh AT, Moore JE, Greenwald SE (2010) Structural inhomogeneity and fiber orientation in the inner arterial media. AJP Hear Circ Physiol 298:H1537–H1545

27. Iliopoulos DC, Kritharis EP, Giagini AT, Papadodima SA, Sokolis DP (2009) Ascending thoracic aortic aneurysms are associated with compositional remodeling and vessel stiffening but not weakening in age-matched subjects. J Thorac Cardiovasc Surg 137:101–109

28. Holzapfel GA, Sommer G, Auer M, Regitnig P, Ogden RW (2007) Layer-Specific 3D Residual Deformations of Human Aortas with Non-Atherosclerotic Intimal Thickening. Ann Biomed Eng 35:530–545

29. Heistad DD, Marcus ML (1979) Role of Vasa Vasorum in Nourishment of the Aorta. J Vasc Res 16:225–238

30. Fung YC, Fronek K, Patitucci P (1979) Pseudoelasticity of arteries and the choice of its mathematical expression. Am. J. Physiol. - Hear. Circ. Physiol. 237:

31. Sun W, Sacks MS (2005) Finite element implementation of a generalized Fung-elastic constitutive model for planar soft tissues. Biomech Model Mechanobiol 4:190–199

32. Baek S, Gleason RL, Rajagopal KR, Humphrey JD (2007) Theory of small on large: Potential utility in computations of fluid-solid interactions in arteries. Comput Methods Appl Mech Eng 196:3070–3078

33. Ferruzzi J, Vorp D a, Humphrey JD (2011) On constitutive descriptors of the biaxial mechanical behaviour of human abdominal aorta and aneurysms. J R Soc Interface 8:435–450

34. Holzapfel GA, Sommer G, Gasser CT, Regitnig P (2005) Determination of layer-specific mechanical properties of human coronary arteries with nonatherosclerotic intimal thickening and related constitutive modeling. Am. J. Physiol. - Hear. Circ. Physiol. 289:

35. Lanir Y (1983) Constitutive equations for fibrous connective tissues. J Biomech 16:1–12

36. Länne T, Sonesson B, Bergqvist D, Bengtsson H, Gustafsson D (1992) Diameter and compliance in the male human abdominal aorta: Influence of age and aortic aneurysm. Eur J Vasc Surg 6:178–184

37. Sonesson B, Länne T, Vernersson E, Hansen F (1994) Sex difference in the mechanical properties of the abdominal aorta in human beings. J Vasc Surg 20:959–969

38. Lederle FA, Johnson GR, Wilson SE, et al (1997) Relationship of age, gender, race, and body size to infrarenal aortic diameter. J Vasc Surg 26:595–601

39. Horny L, Adamek T, Gultova E, Zitny R, Vesely J, Chlup H, Konvickova S (2011) Correlations between age, prestrain, diameter and atherosclerosis in the male abdominal aorta. J Mech Behav Biomed Mater 4:2128–2132

40. Cattell MA, Anderson JC, Hasleton PS (1996) Age-related changes in amounts and concentrations of collagen and elastin in normotensive human thoracic aorta. Clin Chim Acta 245:73–84

41. Franklin SS, Gustin W, Wong ND, Larson MG, Weber MA, Kannel WB, Levy D (1997) Hemodynamic Patterns of Age-Related Changes in Blood Pressure. Circulation 96:

42. Mitchell GF, Parise H, Benjamin EJ, Larson MG, Keyes MJ, Vita JA, Vasan RS, Levy D (2004) Changes in Arterial Stiffness and Wave Reflection With Advancing Age in Healthy Men and Women. Hypertension 43:

43. Rogers WJ, Hu Y-LL, Coast D, Vido DA, Kramer CM, Pyeritz RE, Reichek N (2001) Age-associated changes in regional aortic pulse wave velocity. J Am Coll Cardiol 38:1123–9

44. McEniery CM, Yasmin, Hall IR, Qasem A, Wilkinson IB, Cockcroft JR (2005) Normal Vascular Aging: Differential Effects on Wave Reflection and Aortic Pulse Wave Velocity: The Anglo-Cardiff Collaborative Trial (ACCT). J Am Coll Cardiol 46:1753–1760

45. Shahmirzadi D, Konofagou EE (2014) Quantification of arterial wall inhomogeneity size, distribution, and modulus contrast using FSI numerical pulse wave propagation. Artery Res 8:57–65

46. Li AE, Kamel I, Rando F, Anderson M, Kumbasar B, Lima JAC, Bluemke DA (2004) Using MRI to Assess Aortic Wall Thickness in the Multiethnic Study of Atherosclerosis: Distribution by Race, Sex, and Age. Am J Roentgenol 182:593–597

47. Hayashi K, Handa H, Nagasawa S, Okumura A, Moritake K (1980) Stiffness and elastic behavior of human intracranial and extracranial arteries. J Biomech 13:175–184

48. Horny L, Adamek T, Vesely J, Chlup H, Zitny R, Konvickova S (2012) Age-related distribution of longitudinal pre-strain in abdominal aorta with emphasis on forensic application. Forensic Sci Int 214:18–22

49. Schulze-Bauer CAJ, Mörth C, Holzapfel GA, Mörth C, Holzapfel GA (2003) Passive biaxial mechanical response of aged human iliac arteries. J Biomech Eng 125:395–406

50. Wilson KA, Woodburn KR, Ruckley C V., Fowkes FGR (1997) Expansion rates of abdominal aortic aneurysm: Current limitations in evaluation. Eur J Vasc Endovasc Surg 13:521–526

51. healthfinder.gov - Talk to Your Doctor about Abdominal Aortic Aneurysm. https://healthfinder.gov/HealthTopics/Category/doctor-visits/screening-tests/talk-to-your-doctor-about-abdominal-aortic-aneurysm#the-basics_2. Accessed 24 Jan 2017

52. Svensjö S, Björck M, Gürtelschmid M, Djavani Gidlund K, Hellberg A, Wanhainen A (2011) Low Prevalence of Abdominal Aortic Aneurysm Among 65-Year-Old Swedish Men Indicates a Change in the Epidemiology of the DiseaseClinical Perspective. Circulation 124:

53. Thompson SG, Ashton HA, Gao L, Buxton MJ, Scott RAP (2012) Final follow-up of the Multicentre Aneurysm Screening Study (MASS) randomized trial of abdominal aortic aneurysm screening. Br J Surg 99:1649–1656

54. Howard DPJ, Banerjee A, Fairhead JF, Handa A, Silver LE, Rothwell PM, Oxford Vascular Study (2015) Population-Based Study of Incidence of Acute Abdominal Aortic Aneurysms With Projected Impact of Screening Strategy. J Am Heart Assoc 4:e001926

55. Brown PM, Zelt DT, Sobolev B (2003) The risk of rupture in untreated aneurysms: The impact of size, gender, and expansion rate. J Vasc Surg 37:280–284

56. Kent KC, Zwolak RM, Egorova NN, Riles TS, Manganaro A, Moskowitz AJ, Gelijns AC, Greco G (2010) Analysis of risk factors for abdominal aortic aneurysm in a cohort of more than 3 million individuals. J Vasc Surg 52:539–548

57. Hoornweg LL, Storm-Versloot MN, Ubbink DT, Koelemay MJW, Legemate DA, Balm R (2008) Meta Analysis on Mortality of Ruptured Abdominal Aortic Aneurysms. Eur J Vasc Endovasc Surg 35:558–570

58. Uk T, Aneurysm S, Participants T (1998) Mortality results for randomised controlled trial of early elective surgery or ultrasonographic surveillance for small abdominal aortic aneurysms. Lancet 352:1649–1655

59. Lederle F a, Johnson GR, Wilson SE, et al (2002) Rupture rate of large abdominal aortic aneurysms in patients refusing or unfit for elective repair. JAMA 287:2968–2972

60. Nicholls SC, Gardner JB, Meissner MH, Johansen KH (1998) Rupture in small abdominal aortic aneurysms. J Vasc Surg 28:884–888

61. Gasser TC, Nchimi A, Swedenborg J, Roy J, Sakalihasan N, Böckler D, Hyhlik-Dürr A (2014) A novel strategy to translate the biomechanical rupture risk of abdominal aortic aneurysms to their

equivalent diameter risk: Method and retrospective validation. Eur J Vasc Endovasc Surg 47:288–295

62. Moll FL, Powell JT, Fraedrich G, et al (2011) Management of abdominal aortic aneurysms clinical practice guidelines of the European society for vascular surgery. Eur J Vasc Endovasc Surg. doi: 10.1016/j.ejvs.2010.09.011

63. Brewster DC, Cronenwett JL, Hallett JW, Johnston KW, Krupski WC, Matsumura JS (2003) Guidelines for the treatment of abdominal aortic aneurysms: Report of a subcommittee of the Joint Council of the American Association for Vascular Surgery and Society for Vascular Surgery. J Vasc Surg 37:1106–1117

64. Alexander JJ (2004) The pathobiology of aortic aneurysms. J Surg Res 117:163–175

65. Dobrin PB, Baker WH, Gley WC, et al (1984) Elastolytic and Collagenolytic Studies of Arteries. Arch Surg 119:405

66. Zarins CK, Xu C, Glagov S (2001) Atherosclerotic enlargement of the human abdominal aorta. Atherosclerosis 155:157–164

67. Krettek A, Sukhova GK, Libby P (2003) Elastogenesis in Human Arterial Disease. Arterioscler. Thromb. Vasc. Biol. 23:

68. Vande Geest JP, Sacks MS, Vorp DA (2006) The effects of aneurysm on the biaxial mechanical behavior of human abdominal aorta. J Biomech 39:1324–1334

69. Gasser TC, Gallinetti S, Xing X, Forsell C, Swedenborg J, Roy J (2012) Spatial orientation of collagen fibers in the abdominal aortic aneurysm's wall and its relation to wall mechanics. Acta Biomater 8:3091–3103

70. Tong J, Cohnert T, Regitnig P, Holzapfel GA (2011) Effects of age on the elastic properties of the intraluminal thrombus and the thrombus-covered wall in abdominal aortic aneurysms: Biaxial extension behaviour and material modelling. Eur J Vasc Endovasc Surg 42:207–219

71. Raghavan ML, Webster MW, Vorp DA (1996) Ex vivo biomechanical behavior of abdominal aortic aneurysm: assessment using a new mathematical model. Ann Biomed Eng 24:573–582

72. Thubrikar MJ, Robicsek F, Labrosse M, Chervenkoff V, Fowler BL (2003) Effect of thrombus on abdominal aortic aneurysm wall dilation and stress. J Cardiovasc Surg (Torino) 44:67–77

73. Lee D, Yuki I, Murayama Y, et al (2007) Thrombus organization and healing in the swine experimental aneurysm model. Part I. A histological and molecular analysis. J Neurosurg 107:94–108

74. Karšaj I, Humphrey JD (2009) A mathematical model of evolving mechanical properties of intraluminal thrombus. Biorheology 46:509–527

75. Koole D, Zandvoort HJA, Schoneveld A, Vink A, Vos JA, van den Hoogen LL, de Vries J-PPM, Pasterkamp G, Moll FL, van Herwaarden JA (2013) Intraluminal abdominal aortic aneurysm thrombus is associated with disruption of wall integrity. J Vasc Surg 57:77–83

76. Vorp DA, Lee PC, Wang DHJ, Makaroun MS, Nemoto EM, Ogawa S, Webster MW (2001)

Association of intraluminal thrombus in abdominal aortic aneurysm with local hypoxia and wall weakening. J Vasc Surg 34:291–299

77. Reeps C, Maier A, Pelisek J, Härtl F, Grabher-Meier V, Wall WA, Essler M, Eckstein HH, Gee MW (2013) Measuring and modeling patient-specific distributions of material properties in abdominal aortic aneurysm wall. Biomech Model Mechanobiol 12:717–733

78. Wilson JS, Virag L, Di Achille P, Karšaj I, Humphrey JD Biochemomechanics of Intraluminal Thrombus in Abdominal Aortic Aneurysms. doi: 10.1115/1.4023437

79. Gasser TC, Görgülü G, Folkesson M, Swedenborg J (2008) Failure properties of intraluminal thrombus in abdominal aortic aneurysm under static and pulsating mechanical loads. J Vasc Surg 48:179–188

80. Wang DHJ, Makaroun MS, Webster MW, Vorp DA (2002) Effect of intraluminal thrombus on wall stress in patient-specific models of abdominal aortic aneurysm. J Vasc Surg 36:598–604

81. Polzer S, Gasser TC, Swedenborg J, Bursa J (2011) The impact of intraluminal thrombus failure on the mechanical stress in the wall of abdominal aortic aneurysms. Eur J Vasc Endovasc Surg. doi: 10.1016/j.ejvs.2010.12.010

82. Di Martino ES, Vorp DA (2003) Effect of variation in intraluminal thrombus constitutive properties on abdominal aortic aneurysm wall stress. Ann Biomed Eng 31:804–809

83. Hellenthal FAMVI, Geenen ILA, Teijink JAW, Heeneman S, Schurink GWH (2009) Histological features of human abdominal aortic aneurysm are not related to clinical characteristics. Cardiovasc Pathol 18:286–93

84. Fillinger MF, Raghavan ML, Marra SP, Cronenwett JL, Kennedy FE (2002) In vivo analysis of mechanical wall stress and abdominal aortic aneurysm rupture risk. J Vasc Surg 36:589–597

85. Khosla S, Morris DR, Moxon J V., Walker PJ, Gasser TC, Golledge J (2014) Meta-analysis of peak wall stress in ruptured, symptomatic and intact abdominal aortic aneurysms. Br J Surg 101:1350–1357

86. Polzer S, Gasser TC, Markert B, Bursa J, Skacel P (2012) Impact of poroelasticity of intraluminal thrombus on wall stress of abdominal aortic aneurysms. Biomed Eng Online. doi: 10.1186/1475-925X-11-62

87. Gasser TC, Auer M, Labruto F, Swedenborg J, Roy J (2010) Biomechanical rupture risk assessment of abdominal aortic aneurysms: Model complexity versus predictability of finite element simulations. Eur J Vasc Endovasc Surg 40:176–185

88. Fillinger MF, Marra SP, Raghavan ML, Kennedy FE (2003) Prediction of rupture risk in abdominal aortic aneurysm during observation: Wall stress versus diameter. J Vasc Surg 37:724–732

89. Truijers M, Pol JA, SchultzeKool LJ, van Sterkenburg SM, Fillinger MF, Blankensteijn JD (2007) Wall Stress Analysis in Small Asymptomatic, Symptomatic and Ruptured Abdominal Aortic Aneurysms. Eur J Vasc Endovasc Surg 33:401–407

90. Fung YC (1991) What are the residual stresses doing in our blood vessels? Ann Biomed Eng 19:237–249

91. Takamizawa K, Hayashi K (1987) Strain energy density function and uniform strain hypothesis for arterial mechanics. J Biomech 20:7–17

92. Holzapfel GA, Gasser TC (2007) Computational stress-deformation analysis of arterial walls including high-pressure response. Int J Cardiol 116:78–85

93. Balzani D, Schröder J, Gross D (2007) Numerical simulation of residual stresses in arterial walls. Comput Mater Sci 39:117–123

94. Gasser TC, Schulze-Bauer C a J, Holzapfel G a (2002) A Three-dimensional Finite Element Model for Arterial Clamping. J Biomech Eng 124:355

95. Raghavan ML, Vorp DA (2000) Toward a biomechanical tool to evaluate rupture potential of abdominal aortic aneurysm: Identification of a finite strain constitutive model and evaluation of its applicability. J Biomech 33:475–482

96. Truijers M, Fillinger MF, Renema KW, Marra SP, Oostveen LJ, Kurvers HAJM, Schultzekool LJ, Blankensteijn JD (2009) In-vivo imaging of changes in abdominal aortic aneurysm thrombus volume during the cardiac cycle. J Endovasc Ther 16:314–9

97. Govindjee S, Mihalic P a. (1996) Computational methods for inverse finite elastostatics. Comput Methods Appl Mech Eng 136:47–57

98. de Putter S, Wolters BJBM, Rutten MCM, Breeuwer M, Gerritsen FA, van de Vosse FN (2007) Patient-specific initial wall stress in abdominal aortic aneurysms with a backward incremental method. J Biomech 40:1081–1090

99. Ayres C, Bowlin GL, Henderson SC, Taylor L, Shultz J, Alexander J, Telemeco TA, Simpson DG (2006) Modulation of anisotropy in electrospun tissue-engineering scaffolds: Analysis of fiber alignment by the fast Fourier transform. Biomaterials 27:5524–5534

100. Sander EA, Barocas VH (2009) Comparison of 2D fiber network orientation measurement methods. J Biomed Mater Res - Part A 88:322–331

101. Schriefl AJ, Wolinski H, Regitnig P, Kohlwein SD, Holzapfel G a (2013) An automated approach for three-dimensional quantification of fibrillar structures in optically cleared soft biological tissues. J R Soc Interface 10:20120760

102. Marquez JP (2006) Fourier analysis and automated measurement of cell and fiber angular orientation distributions. Int J Solids Struct 43:6413–6423

103. Fillinger M (2007) Who Should We Operate On and How Do We Decide: Predicting Rupture and Survival in Patients with Aortic Aneurysm. Semin Vasc Surg 20:121–127

104. Maier A, Gee MW, Reeps C, Pongratz J, Eckstein HH, Wall WA (2010) A comparison of diameter, wall stress, and rupture potential index for abdominal aortic aneurysm rupture risk prediction. Ann Biomed Eng 38:3124–3134

105. Vande Geest JP, Wang DHJ, Wisniewski SR, Makaroun MS, Vorp DA (2006) Towards a noninvasive method for determination of patient-specific wall strength distribution in abdominal aortic aneurysms. Ann Biomed Eng 34:1098–1106

106. Geest JP Vande, Schmidt DE, Sacks MS, David A (2009) The effects of anisotropy on the stress analyses of patient- specific abdominal aortic aneurysms. 36:921–932

107. Rodríguez JF, Martufi G, Doblaré M, Finol EA (2009) The effect of material model formulation in the stress analysis of abdominal aortic aneurysms. Ann Biomed Eng 37:2218–2221

108. Sweeting MJ, Thompson SG, Brown LC, Powell JT (2012) Meta-analysis of individual patient data to examine factors affecting growth and rupture of small abdominal aortic aneurysms. Br J Surg 99:655–665

109. Eilaghi A, Flanagan JG, Brodland GW, Ethier CR (2009) Strain Uniformity in Biaxial Specimens is Highly Sensitive to Attachment Details. J Biomech Eng 131:91003

110. Sacks MS (2000) Biaxial mechanical evaluation of planar biological materials. J Elast 61:199–246

111. Cruz Perez B, Tang J, Morris HJ, Palko JR, Pan X, Hart RT, Liu J (2014) Biaxial mechanical testing of posterior sclera using high-resolution ultrasound speckle tracking for strain measurements. J Biomech 47:1151–1156

112. Kahlon A, Hurtig MB, Gordon KD (2015) Regional and depth variability of porcine meniscal mechanical properties through biaxial testing. J Mech Behav Biomed Mater 41:108–114